NASA TECHNICAL NOTE

NASA TN D-3758

NASA TN D-3758

ANALYSIS OF SURFACE ABLATION OF NONCHARRING MATERIALS WITH DESCRIPTION OF ASSOCIATED COMPUTING PROGRAM

by Fred W. Matting and Dean R. Chapman

Ames Research Center
Moffett Field, Calif.

NATIONAL AERONAUTICS AND SPACE ADMINISTRATION • WASHINGTON, D. C. • DECEMBER 1966

NASA TN D-3758

ANALYSIS OF SURFACE ABLATION OF NONCHARRING MATERIALS WITH DESCRIPTION OF ASSOCIATED COMPUTING PROGRAM

By Fred W. Matting and Dean R. Chapman

Ames Research Center
Moffett Field, Calif.

NATIONAL AERONAUTICS AND SPACE ADMINISTRATION

For sale by the Clearinghouse for Federal Scientific and Technical Information
Springfield, Virginia 22151 – Price $2.50

TABLE OF CONTENTS

TABLE OF CONTENTS - Concluded

ANALYSIS OF SURFACE ABLATION OF NONCHARRING MATERIALS

WITH DESCRIPTION OF ASSOCIATED COMPUTING PROGRAM

By Fred W. Matting and Dean R. Chapman
Ames Research Center

SUMMARY

A generalized method is presented for solving the problem of stagnation-point heat transfer and material response for blunt bodies experiencing melting and vaporizing or subliming ablation. The analysis is applicable to wind-tunnel and flight conditions (with body forces taken into account); internal radiation can be considered or the material can be assumed opaque; the analysis can be used for different planets. During entry flights, a body will start in the free-molecule regime, pass through a transitional regime, and finish in the continuum regime of gas dynamics. Approximate equations, rationally obtained, are presented which provide "bridges" between the free-molecule and continuum regimes for such quantities as the convective heating rate, surface shear, heat blockage, and mass loss. Several illustrative examples (including surface chemical reaction cases) show the applications of the analysis. Comparisons with experiment are made where possible. The analysis has been machine programmed for numerical solutions using a finite difference scheme, and a running energy balance is kept as a check on accuracy. Instructions are provided for using the computing program.

INTRODUCTION

The development of heat shields for space vehicles and long-range missiles has motivated a marked increase in the effort to understand the process of ablation. This intensified study is contributing to the understanding of natural ablative phenomena that occur when extraterrestrial bodies enter the Earth's atmosphere. Ablation data obtained in the laboratory, for example, in arc-jet wind tunnels, do not duplicate in any single experiment all the conditions of entry flights; hence, there is need for analytical methods of predicting and explaining the ablative phenomena. Before such methods can be applied, however, their validity and accuracy must be determined by comparing calculated results with results from wind-tunnel tests, with flight data, or with post-flight observations of a man-made or natural object when one can be recovered.

A generalized method is presented here for solving the combined problem of heat transfer and material response for the stagnation region of blunt bodies experiencing melting and vaporizing or subliming ablation. An attempt has been made to describe the problem mathematically as completely as possible in order to obtain nearly exact solutions. This required that the analysis be machine programmed for numerical solutions. This program in various stages of

development has been used successfully at Ames Research Center during the past three years. It has previously been employed in the analysis of tektite ablation (refs. 1, 2).

A number of the equations used in the analysis are already well established (refs. 3-6); however, some of the equations and features of the analysis are new. The analysis takes account of the fact that entry bodies initially fly in the free-molecule regime, then in a transitional regime, and finally in the continuum regime of gas dynamics. The analysis contains formulas for the transitional regime to bridge between the free-molecule and continuum regimes; these formulas have been rationally derived from simple models and are believed to fill an important gap in previous analyses of small objects entering a planetary atmosphere.

Several options in the analysis and associated computing program are available. Internal radiation in the body is accounted for, or the body can be assumed to be opaque. Flight cases as well as wind-tunnel cases can be calculated; the flight cases can be applied to any planet, provided certain characteristics of the atmosphere are known. The rear boundary conditions for the ablating material can be those for a heat shield, or the aerodynamic base heating for an object, such as a tektite, can be accounted for. The ablating material can be a type that melts and/or vaporizes, sublimes, or undergoes a surface chemical reaction in the ablation process. The various material properties and the external flow conditions can be put into the computing program arbitrarily so that a variety of ablation research problems can be studied.

To illustrate the types of problems that can be handled by the analysis (and to elucidate some of the significant ablative phenomena), several typical examples are presented. These are calculated by the numerical computing program associated with the analysis. The principal features of the numerical computing program are described, and instructions are given for its use.

ANALYSIS AND METHOD OF SOLUTION

In this section, the principal emphasis is on the method of solution used in the associated computer program. Equations are presented in specific form with numerical values inserted for universal constants. In performing calculations for various materials and situations, the user has a number of parameters (constants) at his disposal; typical values of these are listed in the description as they appear.

Basic Approach and Approximations

The analysis is concerned with the problem of surface ablation near the stagnation point for transparent or opaque materials of finite thickness. The analysis is thus restricted to materials that undergo surface ablation including melting, evaporation, sublimation, or surface chemical reactions, such as depolymerization. Chemical reactions involving the external gases are not

considered. The boundary-layer equations, as such, are not solved, but results of known solutions are used to obtain heating rates, surface shear, and the effects of mass transfer. Front and back surface heating rates must be solved for, in order to determine the front and back face boundary conditions. Two types of heating environments are treated. One is of constant velocity and stream density, such as generally exists in an arc-heated wind tunnel; the other is of time-varying velocity and density over an entry flight (using a constant lift/drag ratio but a variable mass). In this latter environment, the equations of motion are solved simultaneously with the heat-transfer and ablation equations. In the equations of motion, the ratio of body mass to the product of drag coefficient by frontal area appears, and this is related (empirically) to the surface recession.

Conservation Equations

The analysis is essentially a time-dependent energy balance along the stagnation center line of an axisymmetric blunt body. The basic equations to be solved are the conservation equations for energy, mass, and momentum for the material of the body, written in a simplified form that is valid in the stagnation region. The energy and momentum equations have been further simplified by neglecting inertial terms; this procedure is a valid approximation for viscous ablative materials, such as glass, stone, or any subliming material. The curvilinear coordinate system used is shown in sketch (a). The conservation equations are:

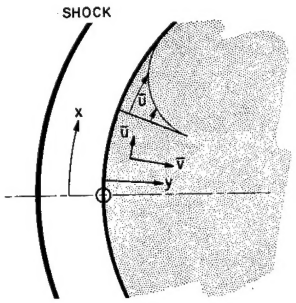

Sketch (a)

Energy

$$\rho c \left(\frac{\partial T}{\partial t} + \bar{v} \frac{\partial T}{\partial y} \right) = \frac{\partial}{\partial y} \left[K \frac{\partial T}{\partial y} - F(y,t) \right] \tag{1}$$

where $F(y,t)$ is the internal radiation flux term.

Continuity (for constant density)

$$\frac{\partial \bar{u}}{\partial x} + \frac{\bar{u}}{x} + \frac{\partial \bar{v}}{\partial y} = 0 \tag{2}$$

x Momentum

$$\frac{\partial}{\partial y} \left(\mu \frac{\partial \bar{u}}{\partial y} \right) = \frac{\partial p}{\partial x} - \frac{\rho a x}{R} \tag{3}$$

Most previous analyses have taken account of internal radiation or vehicle acceleration, but not both. The acceleration term in the momentum equation (3) can be important in determining the rate of removal of melted material; this term, as written, is valid in the stagnation region.

The continuity and momentum equations can be put into quadrature form. We make use of the fact that $\bar{u}$ varies linearly with x near the stagnation center line, and we define: $\bar{\bar{u}} = (\partial\bar{u}/\partial x)_{x=0}$. Then, near the center line

$$\bar{u} = \bar{\bar{u}}x \tag{4}$$

The continuity equation in quadrature form is:

$$\bar{v} = \bar{v}_w - 2\int_0^y \bar{\bar{u}}\, dy_1 \tag{5}$$

The value of $\bar{v}_w$ depends on surface temperature and external conditions; its evaluation is described below in the section, Front Face Velocity. The surface recession rate and surface recession are, respectively,

$$\bar{v}_{sr} = \frac{dX}{dt} = |\bar{v}_{BF}| = |\bar{v}(y_{BF},t)| \tag{6a}$$

$$X = \int_{t_i}^{t} |\bar{v}_{BF}|\, dt_1 \tag{6b}$$

Pressure Gradient

The solution to equation (5) can be substituted into equation (1), but to solve equation (5) we must first obtain $\bar{\bar{u}}(y,t)$ from the momentum equation. We write, for the pressure near the center line,

$$p = p(0) + \frac{1}{2}\, p''(0)x^2 \tag{7}$$

and equation (3) becomes, after substituting equation (4),

$$\frac{\partial}{\partial y}\left(\mu\, \frac{\partial\bar{\bar{u}}}{\partial y}\right) = p''(0) - \frac{\rho a}{R} = -\rho'' \tag{8}$$

where ρ'' is then the negative of the second derivative of pressure with a correction for the body force acting on the material. We can integrate equation (8) twice and obtain:

$$\bar{\bar{u}}(y,t) = \rho'' \int_y^{y_{BF}} \frac{y_1 dy_1}{\mu} + \tau_w' \int_y^{y_{BF}} \frac{dy_1}{\mu} \tag{9}$$

where τ_w' (dynes/cm^3) is the x derivative of the absolute value of the surface shear, $(d\tau_w/dx)_{x=0}$. In ρ'' the quantity, a, is the acceleration of a body in flight (positive for increasing speed). For wind-tunnel calculations

$a = -g$ for a vertical wind tunnel with upward flow and $a = 0$ for a horizontal wind tunnel. In the calculations to be made, $\wp''$ (dynes/cm^4) is evaluated as follows:

Wind tunnel:

$$\wp'' = (A_2 - E_{15}R)\left(\frac{2\times10^4 DV_\infty{}^2}{R^2}\right) \tag{10a}$$

Flight:

$$\wp'' = \left[A_2 - \frac{\rho R}{4\left(\frac{M}{C_D A}\right)}\right]\left(\frac{2\times10^4 DV_\infty{}^2}{R^2}\right)\bar{K}_{tu} \tag{10b}$$

where A_2 (approximately unity) is a correction used with a modified Newtonian approximation,

$$\frac{du_e}{dx} = \frac{V_\infty}{R}\sqrt{\frac{2A_2}{\rho_{21}}} \tag{11}$$

and E_{15} in equation (10a) is selected to give the wind-tunnel body force. The quantity, $\bar{K}_{tu}$, is an empirical correction for oscillation or tumbling in flight. It is evaluated as

$$\bar{K}_{tu} = \bar{K} + (1 - \bar{K})\left[1 - e^{-(X/X_1)^{E_{16}}}\right] \tag{12}$$

where $\bar{K}$ is the fractional time that the center point is initially exposed to approximately stagnation conditions, and X_1 and E_{16} are values selected to give a realistic damping to the oscillation during entry. Typical values for the constants that have been used for calculating a tumbling tektite entry are: $\bar{K} = 0.25$; $X_1 = R/10$ cm; $E_{16} = 1.0$. For a nontumbling body, $\bar{K}$ is unity and the other constants have no influence.

Surface Convective Heat Transfer

In order to evaluate the x gradient of wall shear, τ_w', we require first an evaluation of the surface convective heat transfer; we also need this to determine the surface boundary conditions. Instead of enthalpy (cal/g), we use an "enthalpy velocity" (km/sec), which is defined as

$$V^2 = 0.00836\, h_s \tag{13a}$$

$$V = 0.0915\sqrt{h_s} \tag{13b}$$

For the external gas we use an average specific heat,

$$\bar{c}_p = \frac{1}{T} \int_o^T c_p dT_1 \tag{14}$$

In laminar continuum flow we can evaluate the surface convective heat transfer as (ref. 7) (with a vorticity correction)

$$q_{oc} = A_4 \sqrt{\frac{D}{R}}\, V^{1.15}(V^2 - 0.00836\, \bar{c}_p T_w) \left(1 + \frac{C_6}{\sqrt{DVR}}\right) \tag{15}$$

where A_4 is a constant and C_6 is a vorticity correction (generally small). The results of equation (15) agree well with existing experimental data over an extended range of enthalpy potentials. The value of A_4 for Earth entries is approximately 1.1; in wind-tunnel tests, A_4 is evaluated with a calorimeter. With a blowing correction we have

$$q_{\psi c} = \psi q_{oc} \tag{16}$$

where ψ is evaluated in equation (28).

For high altitude flight or for rarefied wind-tunnel conditions, it is necessary to consider the free-molecule regime. For surface convection in the free-molecule regime we use a Newtonian type of approximation (ref. 8, pp. 395-403).

$$q_{FM} = \frac{A_{cq} D V_\infty}{0.0836} (V^2 - 0.00836\, \bar{c}_p T_w) \tag{17}$$

In the transition regime between free-molecule and continuum flow, the convective heat transfer will have a value bridged between the evaluations in equations (16) and (17). This has been derived from a simple kinetic theory model (see appendix C) yielding the result

$$q_{\psi w} = q_{\psi c} \left(1 - e^{-q_{FM}/q_{\psi c}}\right) \tag{18}$$

When the tumbling correction is applied, the convective heat transfer at the front wall is

$$q_w = q_{\psi w} \bar{K}_{tu} \tag{19}$$

Equations (15) to (19) are used to determine the convective heat transfer to the front face, but it is also of interest to calculate some related quantities. When no material is being lost to the vapor state, $\psi = 1$, and

equation (18) specializes to

$$q_{oo} = q_{oc}\left(1 - e^{-q_{FM}/q_{oc}}\right) \tag{20}$$

and equation (19) specializes to

$$q_o = q_{oo}\bar{K}_{tu} \tag{21}$$

When material is lost to the vapor state, $\psi \neq 1$; we can consider that ψ operates on q_{oc} but not on q_{FM}. Then a modified ψ can be obtained to operate on q_{oo}. We define the modified blowing factor, $\bar{\psi}$, as:

$$\bar{\psi} = \frac{q_{\psi w}}{q_{oo}} \tag{22a}$$

$$q_{\psi w} = \bar{\psi} q_{oo} \tag{22b}$$

On multiplying both sides of equation (22b) by $\bar{K}_{tu}$, we have also

$$q_w = \bar{\psi} q_o \tag{23}$$

When we substitute equations (16), (18), and (20) into (22a), the evaluation of $\bar{\psi}$ becomes

$$\bar{\psi} = \frac{\psi\left(1 - e^{-q_{FM}/\psi q_{oc}}\right)}{1 - e^{-q_{FM}/q_{oc}}} \tag{24}$$

Equations (20) to (24) are alternate forms entirely equivalent to equations (18) and (19). The quantities q_{oo}, q_o, and $\bar{\psi}$, although not needed in determining the convective heat transfer, are computed as quantities of interest conceptually.

The bridging relation given in equation (18) or the alternate forms in equations (20) and (24) will automatically take account of changes of heating rates as a body flies from one regime into another and will place control in the appropriate regime. Comparisons with available measured data are shown in appendix C.

For normal (nonrarefied) wind-tunnel conditions, the bridging relations given above are not needed; also there is no tumbling, so we have simply:

$$\bar{K}_{tu} = 1 \tag{25a}$$

$$\bar{\psi} = \psi \tag{25b}$$

$$q_o = q_{oc} \tag{25c}$$

$$q_w = \psi q_o \tag{25d}$$

In the heat-transfer relations given above from equation (15) to equation (25), the blowing parameter, ψ, is needed. To evaluate ψ, we need to know the relationship between the equilibrium vapor pressure and temperature for the ablating material, $p_{ve} = p_{ve}(T_w)$. We will write

$$P = \frac{p_{t_2}}{p_{vm}} - 1 = \left[\frac{p_{t_2}}{p_{ve}(T_w)}\right]^{E_7} - 1 \tag{26}$$

where p_{vm} is the modified equilibrium vapor pressure when the equilibrium is shifted by the presence of other gaseous materials in the boundary layer. An example of this is the suppression of vaporization of silica due to the presence of oxygen in the atmosphere. This suppression effect for silica is analyzed in reference 9 in which an analytic, but implicit, expression is obtained for the modified equilibrium vapor pressure. The use of the exponent, E_7, is an empirical accounting for this effect which yields values within several percent of the values obtained by the rigorous analysis of reference 9. For silica, the value $E_7 = 1.4$ has been used. For a number of other materials, $E_7 = 1$, or the modified equilibrium vapor pressure is the usual equilibrium value. For p_{t_2} (in atmospheres) we use a hypersonic approximation (twice the free-stream dynamic pressure with a correction factor):

$$p_{t_2} = \frac{A_1 D V^2}{101.3} \tag{27}$$

where a typical value for A_1 is 0.95, and the number, 101.3, accounts for the units in the equation. Equation (26) is a limiting form for continuum conditions; P could be based on the actual existing vapor pressure, p_v, which will not be an equilibrium value, but in the limit p_v approaches p_{vm} from below. However, p_v cannot exceed p_{t_2}, so for this equation, whatever value p_{vm} may actually take, it is not allowed to exceed p_{t_2} in equation (26). This has been done by giving P a lower limit which is a small positive number (10^{-6}). So P is defined by equation (26) down to its lower limit. The quantities, p_v, p_{ve}, p_{vm}, p_{t_2}, and P, are considered to be evaluated at the liquid or solid surface.

We can represent ψ for an evaporation or sublimation process as

$$\psi = \frac{1 - E_{35}}{1 + \frac{B_{11}}{P}} + E_{35} \tag{28a}$$

This relation, with the asymptote, $E_{35} = 0.06$, gives a good fit to a number of boundary-layer solutions (refs. 10-12). Equation (28a) is also a limiting form for continuum conditions since P, as evaluated in equation (26), is not based on the actual vapor pressure, p_v. The quantity $1/P$ is a function of the mass loss rate due to vaporization (see eqs. (38), (39a), and (40) below). For a surface chemical reaction we use the form

$$\psi = \frac{1 - E_{35}}{1 + \dfrac{B_{11}}{P[1 + (\bar{v}_{wc}/\bar{v}_{wFM})]}} + E_{35} \tag{28b}$$

where $\bar{v}_{wc}$ and $\bar{v}_{wFM}$ are shown evaluated velow in equations (38) and (39e). The correction using $\bar{v}_{wc}$ and $\bar{v}_{wFM}$ takes account of the possible reaction rate control of the mass loss rate which does not depend on the (modified) equilibrium vapor pressure (eqs. (39e) and (40)). The quantity, B_{11} in equation (28) (0.95-1.55 used), depends on the ratio of molecular weights of external gas to blowing gas and should preferably be determined by experiment. In the absence of experiment, we can estimate B_{11} as follows. We can define

$$\bar{M} = \frac{m_e}{m_v} \tag{29}$$

and we have

$$B_{11} = \frac{\text{constant}}{\bar{M}^n} \tag{30}$$

where the constant ≈ 0.7 to 0.8 and $n \approx 2/3$ to $3/4$.

Wall Shear Gradient

We are now in position to evaluate the x gradient of the wall shear, $\tau_w' = (d\tau_w/dx)_{x=o}$. We first consider the case of continuum flow with no blowing to evaluate $\tau_o' = (d\tau_o/dx)_{x=o}$. Using a modified form of Reynolds analogy, we can write:

$$\frac{q_{oc}}{\Delta h} = \frac{K_\sigma \tau_o'}{10^5 \left(\dfrac{du_e}{dx}\right)_{x=o}} \tag{31}$$

where K_σ is a constant that depends on the Prandtl number and is unity when the Prandtl number is unity. Using equation (11) we obtain

$$A_3 = \frac{\sqrt{2A_2}}{K_\sigma} = \frac{\tau_o' R \sqrt{\rho_{21}}\ (\Delta h)}{10^5 q_{oc} V_\infty} \tag{32a}$$

$$\tau_o' = \frac{A_3 q_{oc} V_\infty 10^5}{R(\Delta h)\sqrt{\rho_{21}}} \tag{32b}$$

where $A_3 \approx 1.45$ is a typical value. We apply the tumbling or oscillation correction, $\bar{K}_{tu}$, (eq. (12)) to τ_o' and obtain

$$\tau_{oc}' = \tau_o' \bar{K}_{tu} \tag{33}$$

For the effect of blowing on wall shear in continuum flow we use (ref. 11)

$$\frac{\tau_{wc}'}{\tau_{oc}'} = \psi \left(1 + \frac{E_8}{P} \psi\right) \tag{34}$$

The value of E_8 should be small; unless experimental evidence is available, it is suggested that the value zero be used. (Reasonable answers have also been obtained with $E_8 = 0.3\ B_{11}$.) In the numerical computing program, the value of P that is inserted into equation (34) (only) is arbitrarily prevented from becoming less than E_8 so that the shear blowing factor cannot become unrealistically large when the actual P is very small. Using equations (32b, 33, and 34), we obtain our expression for τ_{wc}' in continuum flow.

$$\tau_{wc}' = \frac{836 A_3 q_{oc} V_\infty \bar{K}_{tu} \psi [1 + (E_8/P)\psi]}{R\sqrt{\rho_{21}}\ (V^2 - 0.00836\ \bar{c}_p T_w)} \tag{35}$$

For the x gradient of shear in free molecule flow (which is unaffected by blowing), we have (ref. 8, pp. 395-403)

$$\tau_{wFM}' = \frac{A_{cm} D V_\infty^2 10^4 \bar{K}_{tu}}{R} \tag{36}$$

where A_{cm} is the x momentum accommodation coefficient. For the bridging between free-molecule and continuum wall shear, we use essentially the same model as that used for heat-transfer bridging (see appendix C).

$$\tau_w' = \tau_{wc}' \left(1 - e^{-\tau_{wFM}'/\tau_{wc}'}\right) \tag{37}$$

The evaluations of ρ'' and τ_w' given above along with knowledge of the temperature distribution enable us to solve equation (9) for $\bar{\bar{u}}(y,t)$ which can be substituted into equation (5).

Front Face Velocity

To solve equation (5) we need to evaluate the front face velocity, $\bar{v}_w$. For the front face velocity under continuum conditions, we use the so-called Lewis analogy (Le = 1), which states that the ratio of mass diffusion to concentration "gradient" is equal to the ratio of continuum heat transfer to enthalpy potential:

$$|\bar{v}_{wc}| = \frac{0.00836\ \psi q_{oc}}{\rho \bar{M} P (V^2 - 0.00836\ \bar{c}_p T_w)} \tag{38}$$

An equivalent form of equation (38) is given as equations (31) and (32) of reference 9 (see also ref. 13). Equation (38) is a limiting form for continuum conditions, because of the way P is evaluated in equation (26). (As noted previously, P is evaluated at the solid or liquid surface.) Equation (38) also contains empiricism in the evaluation of ψ (eq. (28)). In reality, it is expected that the diffusion rate should reach a maximum value with a very small P, if P were based on the actual pressure at the surface, p_v. This would also require that the ψ asymptote be zero. With a finite ψ asymptote (which seems to fit existing data), the calculated diffusion rate becomes unrealistically large for small P. Under these conditions it can be expected that free-molecule or reaction-rate control will generally prevail (see eq. (40)), so that an inaccurate calculation of the diffusion rate for these conditions will have little effect on the net rate calculated.

For the calculation of the front face velocity in the free-molecule or rate-controlled regime, we distinguish two cases: (1) evaporation or sublimation, and (2) a chemical reaction such as a depolymerization. For the evaporation or sublimation case, we have, from kinetic theory, the Langmuir equation (C1). With constants evaluated to account for our units we have:

$$|\bar{v}_{wFM}| = \frac{44.3 A_{cv} p_{ve}}{\rho} \sqrt{\frac{m_v}{T_w}} \tag{39a}$$

Using equation (29) we write

$$|\bar{v}_{wFM}| = 239 \left(A_{cv} \sqrt{\frac{m_e}{29.1}} \right) \frac{p_{ve}}{\rho \sqrt{\bar{M} T_w}} \tag{39b}$$

We now use

$$A_{cv}' = A_{cv} \sqrt{\frac{m_e}{29.1}} \tag{39c}$$

and get

$$|\bar{v}_{wFM}| = \frac{239 A_{cv}' p_{ve}}{\rho \sqrt{\bar{M} T_w}} \tag{39d}$$

Equation (39d) is the form we use in our calculations. When the molecular weight m_e of the external gas is 29.1, the accommodation coefficient can be used directly in equation (39d); otherwise the accommodation coefficient must be corrected according to equation (39c).

For the chemical reaction case, we use an Arrhenius rate form for a first order reaction

$$\left|\overline{v}_{wFM}\right| = Be^{-E_T/T_w} \tag{39e}$$

In the coordinate system used, both $\overline{v}_{wc}$ and $\overline{v}_{wFM}$ will be negative quantities. The bridging equation between the free-molecule or reaction-rate controlled regime and the continuum or diffusion controlled regime turns out to be (see appendix C):

$$\frac{1}{\overline{v}_w} = \frac{1}{\overline{v}_{wFM}} + \frac{1}{\overline{v}_{wc}} \tag{40a}$$

$$\overline{v}_w = \frac{\overline{v}_{wFM}\overline{v}_{wc}}{\overline{v}_{wFM} + \overline{v}_{wc}} \tag{40b}$$

The use of equation (40) automatically places the front face velocity in the appropriate controlling regime: the diffusion-controlled, the rate-controlled, or the transitional regime.

Internal Radiation

In the energy equation (1), we require the evaluation of the internal radiative flux, $F(y,t)$. In the evaluation of F, we assume either an opaque body ($F \equiv 0$) or a transparent gray body (two shades of gray; one for the incoming gas cap radiation, another for the absorption-emission of the heat-shield material). A third alternative is to approximate the transparent gray body by a semitransparent body that is opaque internally, but has a variable surface emissivity.

The evaluation of the radiative flux for the gray transparent body is given below; it is similar to that of reference 14 which treats scattered radiation and uses an exponential attenuation. The present evaluation considers one reflection from the front and the rear surfaces, which is a good approximation for materials that absorb well.

$$\frac{F(y,t)}{2n^2\alpha\sigma} = \int_0^y T^4(\eta)E_2[\alpha(y - \eta)]d\eta - \int_y^{y_{BF}} T^4(\eta)E_2[\alpha(\eta - y)]d\eta$$

$$+ R_{eff} \int_0^{y_{BF}} T^4(\eta)\{E_2[\alpha(y + \eta)] - E_2[\alpha(2y_{BF} - (y + \eta))]\}\, d\eta$$

$$+ \frac{q_R}{2n^2\alpha\sigma}\left[e^{-\alpha_2 y} - R_{eff}e^{-\alpha_2(2y_{BF}-y)}\right] \tag{41}$$

R_{eff} is the effective coefficient of reflection for planar radiation and is related to the maximum emissivity by the relationship (ref. 15)

$$1 - R_{eff} = \frac{\epsilon_{max}}{n^2} \tag{42}$$

The second-degree exponential integral $E_2(z)$, used as the attenuation function in the integrals of equation (41), is (ref. 16, appendix I):

$$E_2(z) = \int_1^\infty \frac{e^{-zx_1}}{x_1^2}\, dx_1 = \int_0^1 e^{-z/\mu_1}\, d\mu_1 \tag{43}$$

In actual numerical calculations, equation (41) is used directly to evaluate F at the front and back faces only. The quantity, $g = \partial F/\partial y$, is obtained by taking the derivative of equation (41), and g is numerically evaluated for use in equation (1). Internal values of F are then obtained by numerical quadrature of the flux derivative, g. The gas cap radiative flux, q_R, is evaluated with an empirical approximation:

$$q_R = E_4 R D^{E_5} V^{E_6} \bar{K}_{tu} \tag{44}$$

The form of equation (44) is deduced from experimental correlations presented in reference 17. Input constants E_4, E_5, and E_6 for a given environment should be selected to fit available data. The level of radiation and the surface reflectivity are both accounted for in the evaluation of E_4; E_5 can vary from 0.5 for nonequilibrium radiation to 1.7 for equilibrium radiation in air, while E_6 can vary from 5 to 8 for air. After the exponents are selected, E_4 should be chosen to give the proper level of radiation. Values of the constants that have been used for Earth tektite entries are: $E_4 = 0.76\times10^{-6}$; $E_5 = 0.5$; $E_6 = 7.0$.

In the calculation for a semitransparent body, the material is considered to be internally opaque, and the front surface emissivity is varied in an appropriate manner with the thermal thickness of the temperature profile. This variation is derived by assuming an exponential temperature distribution

near the wall. This permits a closed form integration, and the result is further approximated to the following simple form:

$$\epsilon_{FF} = \frac{\epsilon_{max}}{1 + \frac{2.4}{\alpha\Delta}} = \frac{\epsilon_{max}}{1 + \frac{E_{33}}{\Delta}} \tag{45}$$

where $E_{33} = 2.4/\alpha$ and the thermal thickness, Δ, is evaluated in equation (63). (If $(\partial T/\partial y)_w \geq 0$ or $\Delta \leq 0$, then ϵ_{FF} is assigned the value of ϵ_{max}.) With this representation, the back-face emissivity ϵ_{BF} is assumed to be constant and $F \equiv 0$. The semitransparent approximation gives virtually the same results for most ablation characteristics as the transparent case (see table I), although the internal temperature profiles do not agree closely. It greatly reduces computing machine time, however; hence it is used for most calculations when an accuracy of the order of 10 percent is adequate.

Boundary Conditions

The evaluations of all the terms in the energy equation (1) have been shown, so this equation is in a form to be solved for $T(y,t)$. Boundary conditions are needed for equation (1), and these are determined in the standard manner by writing surface energy balances for the front and back surfaces, providing for the appropriate differences between the opaque and transparent cases. Options are provided in determining the rear surface boundary conditions as shown below.

The energy balance for the front surface is written:

$$-\left(K \frac{\partial T}{\partial y}\right)_w = \rho h_v \bar{v}_w + q_w + (1 - B_{16})(q_R - \epsilon_{FF}\sigma T_w^4) \tag{46}$$

where

$B_{16} = 0$ for the opaque and semitransparent cases

$B_{16} = 1$ for the transparent case

In the coordinate system used, the front face remains at the origin. As material is lost, the location of the back face recedes to smaller values of y_{BF}, or the region in which we are solving equation (1) becomes smaller. So, to know the location of the back face, at any time, t, the system of equations must have been solved up to time, t.

In writing the back surface energy balance, we distinguish between a back surface exposed to flight conditions and a back surface in contact with a backing material. For the back surface exposed to flight conditions (as, for example, with a tektite), we write the following back surface energy balance:

$$\left(K \frac{\partial T}{\partial y}\right)_{BF} = q_{BF} + (B_{16} - 1)\epsilon_{BF}\sigma(T_{BF}^4 - T_o^4) \tag{47}$$

where B_{16} is zero or unity as noted above. The back surface convective heat transfer, q_{BF}, may be a function of surface temperature. We relate q_{BF} to the front surface convective heat transfer (without blowing), q_o, empirically as follows:

$$\frac{q_{BF}}{(h_s - h_{BF})} = \frac{R_{B/F} q_o}{(h_s - h_w)} \left[1 + (E_{19} - 1)\left(1 - e^{-E_{13} D V_\infty R_b}\right)\right] \tag{48}$$

where $R_{B/F}$ is defined as the ratio of base to front-face laminar convective heating when normalized by the respective enthalpy potentials. To account for transition to turbulent flow at the base, we use:

$$E_{19} = \frac{q_{BF\ turbulent}}{q_{BF\ laminar}} \tag{49}$$

$$E_{13} = \frac{0.2}{\mu_\infty Re_{transition}} = \frac{0.2}{\mu_\infty \left[\frac{(D10^{-6})(V_\infty 10^5) 2R_b}{\mu_\infty}\right]_{transition}} = \frac{1}{(DV_\infty R_b)_{at\ transition}} \tag{50}$$

Typical values of constants that have been used for tektite entries are: $R_{B/F} = 0.01$; $E_{13} = 0.01$; $E_{19} = 5.0$. When the quantities, $R_{B/F}$ and ϵ_{BF}, are assigned the value zero, the back boundary condition is adiabatic.

For numerical computations of the transparent case, the computing program has been arranged so that it is possible to modify equations (46) and (47) by assigning some radiant energy to the surface energy balances. The reasons for this are explained in the section, METHOD OF THE NUMERICAL PROGRAM, Boundary Conditions for the Transparent Case, equations (97) and (98).

The other back boundary condition of interest is used for heat-shield calculations. We assume a backing material which acts as a heat sink and is at uniform (but increasing) temperature, T_{BF}. For an opaque heat shield the heat transfer is entirely by conduction to the backing material; for a transparent heat shield, we assume that, in addition to conduction, the radiative flux, $F(y_{BF},t)$ is entirely absorbed by the backing material. Then, in place of equations (47) to (50) we write

$$\bar{c}\left(\frac{\partial T}{\partial t}\right)_{BF} = -\left(K \frac{\partial T}{\partial y}\right)_{BF} + B_{16} F(y_{BF},t) \tag{51}$$

where $\bar{c}$ is the heat capacity per unit area of the backing material. In the limiting case with $\bar{c} = 0$, the back boundary condition is adiabatic, and

equation (51) should be replaced by equations (47) and (48) with $R_{B/F}$ and ϵ_{BF} assigned the value zero.

It should be noted that the surface temperatures generally cannot be specified a priori, as they depend partly on external conditions that may change with time. The computing program must "find" the appropriate boundary conditions that satisfy the partial differential equation (1) and the surface energy balances.

Trajectory Equations

For flight we must solve simultaneously the conservation equations and the trajectory equations of motion. We use the two-dimensional trajectory equations (with variable mass) for entry in a meridional plane, as shown below (ref. 18).

$$V_\infty = \sqrt{u^2 + v^2} \tag{52a}$$

$$\gamma = \tan^{-1}\left(\frac{v}{u}\right) \tag{52b}$$

$$\frac{du}{dt} = -\frac{DV_\infty}{20\left(\frac{M}{C_D A}\right)}\left[u + \left(\frac{L}{D_r}\right)v\right] - \frac{uv}{R_p} \tag{53a}$$

$$\frac{dv}{dt} = \frac{u^2}{R_p} - \frac{g_p}{10^5} - \frac{DV_\infty}{20\left(\frac{M}{C_D A}\right)}\left[v - \left(\frac{L}{D_r}\right)u\right] \tag{53b}$$

$$\frac{dD}{dt} = \frac{-Dv}{S_h} \tag{54}$$

We also use a hypersonic approximation that considers the ambient atmospheric enthalpy to have a constant value:

$$V = \sqrt{V_\infty{}^2 + E_{38}} \tag{55a}$$

$$E_{38} = 0.00836\ h_\infty \tag{55b}$$

where h_∞ is the effective average constant atmospheric enthalpy in cal/g, and E_{38} (an input to the computing program) has the units km^2/sec^2. For Earth entries, 0.5 has been used for E_{38}.

Equations (53) and (54) can be solved numerically in a straightforward manner. As programmed, L/D_r has been taken as constant for a given body. The atmospheric scale height, S_h, has been programmed so that it may change at selected values of atmospheric density, D. One computing option for Earth entries provides automatic changes in S_h through three values to represent the ARDC atmosphere. For arbitrary planet entries, four arbitrary successive values of S_h can be used. (See appendix D.)

The quantity, M/C_DA (g/cm^2), must be evaluated for use in equation (53). The variation of M/A has been set up empirically as a function of the surface recession, χ. This is equivalent to assuming a geometry for the recession shape:

$$\frac{M}{A} = \left(\frac{M}{A}\right)_i \left[1 + E_{18}\chi + C_3\left(e^{C_4\chi} - 1\right)\right] \tag{56}$$

The variation of the drag coefficient, C_D, through the free-molecule, transitional, and continuum regimes, is represented by a bridging equation developed in appendix C:

$$C_D = C_{DC}\left[1 + E_9 e^{-15(RD)(1+E_{14})}\right] \tag{57}$$

where

$$E_9 = \frac{C_{DFM} - C_{DC}}{C_{DC}} \tag{58}$$

and E_9 depends on the body shape. The free-molecule drag coefficient, C_{DFM}, may be given the value 2. The parameter, E_{14}, has some dependence on body shape (and flight conditions), but will often be assigned the value zero (the value for a sphere in air). We combine equations (56) and (57) to obtain

$$\frac{M}{C_DA} = \left(\frac{M}{C_{DC}A}\right)_i \frac{\left[1 + E_{18}\chi + C_3\left(e^{C_4\chi} - 1\right)\right]}{\left[1 + E_9 e^{-15(RD)(1+E_{14})}\right]} \tag{59}$$

In this equation, C_{DC} is shown grouped with the initial value of $M/C_{DC}A$, because this initial quantity is used in the computing program. The empiricism in equation (59) can also be used to account for any change in C_{DC} with change of body shape.

Miscellaneous Relations

Nose radius.- The effective nose radius, R, is calculated as a quantity that has an empirical variation with the surface recession.

$$R = R_i \left[1 + E_{17} X^2 + C_1 \left(e^{C_2 X} - 1 \right) \right] \tag{60}$$

It is desirable to evaluate the constants in equation (60) from experimental data. Otherwise, one must estimate the geometrical shape of the ablation surfaces.

Density ratio across normal shock.- In several of the relations presented, the density ratio across a normal shock, ρ_{21}, appears. For wind-tunnel calculations, ρ_{21} is considered to remain constant for a particular case. The value of ρ_{21} is a portion of the input data for these cases. For flight calculations, ρ_{21} changes and must be continuously calculated. For flight cases we use the equations:

$$\rho_{21} = \frac{\rho_2}{\rho_\infty} = \left(\frac{\rho_2}{\rho_\infty} \right)_{eq} - E_{11} \left[\left(\frac{\rho_2}{\rho_\infty} \right)_{eq} - 6 \right] e^{-E_{12} R V^5 D} \tag{61}$$

$$\left(\frac{\rho_2}{\rho_\infty} \right)_{eq} = \left(18 - 12 e^{\frac{2-V}{3}} \right) \left[1 + 0.08 \log_{10} \left(\frac{0.1226}{D} \right) \right] \tag{62}$$

Equations (61) and (62) are empirical relations that give good fits to data for air. Equation (61) accounts for nonequilibrium effects, while equation (62) fits equilibrium air data, such as presented in reference 19. The equations provide a valid approximation for any gas mixture that consists predominantly of nitrogen. The entire analysis is not overly sensitive to the evaluation of ρ_{21}. It appears as a square root in equations (11) and (35) which are approximations themselves. Values of E_{11} and E_{12} that have been used for Earth entries are 1.0 and 0.0001, respectively.

Other Calculated Quantities

Although not always required in the analysis described in the preceding subsections, several other quantities are calculated because they are of interest. These are described below.

Thermal thicknesses.- We calculate the thermal thickness, Δ, based on the wall temperature gradient.

$$\Delta = \frac{-(T_W - T_O)}{(\partial T / \partial y)_W} \tag{63}$$

This is meaningful only when $(\partial T/\partial y)_W < 0$ (otherwise Δ is arbitrarily assigned the value 10^6). We also calculate a viscosity thickness, Δ_μ, which we define as the depth at which $\mu = e\mu_W$. The corresponding viscosity thickness temperature is T_{Δ_μ}. The quantity, T_{Δ_μ}, is determined from T_W and the viscosity representation formula, equation (85), below. The quantity, Δ_μ, is determined by interpolation of temperature profile data. If $(\partial T/\partial y)_W \geq 0$ or if T_{Δ_μ} exists nowhere in the temperature profile, Δ_μ is assigned the value zero.

Stored energy comparison with exponential temperature profile.- Using a quantity, φ, we compare each calculated temperature profile with an exponential profile having the same $(\partial T/\partial y)_w$. The quantity φ is defined as the ratio of energy stored to the stored energy associated with the corresponding exponential temperature profile (with form similar to equation (A1) in appendix A). Both energies are calculated as constant property approximations. For the area under the exponential profile we have:

$$A_{exp} = \Delta(T_w - T_o)\left(1 - e^{-y_{BF}/\Delta}\right)(1 + R_{B/F}) \approx \Delta(T_w - T_o)$$

Then,

$$\varphi = \frac{\int_o^{y_{BF}} (T - T_o)\,dy_1}{\Delta(T_w - T_o)} \tag{64}$$

Removal of melted material by pressure gradient and surface shear.- We calculate a term that compares the removal of melt by the pressure gradient and the surface shear. We define the quantity, A_{2D}, as an approximate evaluation of twice the ratio of the portion of the melting velocity, $\bar{\bar{u}}x$, due to the pressure gradient to that due to surface shear. The exact quantity would be twice the ratio of the first term to the second term in equation (9), at $y = 0$. However, we use the approximation, $\mu \approx \mu_w e^{(y/\Delta_\mu)}$, in the integrals and obtain the simple approximate expression,

$$A_{2D} = \frac{2\rho''\Delta_\mu}{\tau_w'} \tag{65}$$

Surface recession due to vaporization and melting.- We are interested in comparing the surface recession due to vaporization with that due to melting. We define $\bar{F}$ as the instantaneous ratio of the surface recession rate due to vaporization to the total surface recession rate (due to vaporization and melting).

$$\bar{F} = \frac{\bar{v}_w}{\bar{v}_{BF}} \tag{66}$$

For the ratio of the surface recession due to vaporization to the total surface recession at any time, t:

$$\bar{F}_t = \frac{\int_{t_i}^{t} |\bar{v}_w|\,dt_1}{\int_{t_i}^{t} |\bar{v}_{BF}|\,dt_1} = \frac{\int_{t_i}^{t} |\bar{v}_w|\,dt_1}{\chi} = \frac{\chi_{vap}}{\chi} \tag{67}$$

Flow lines in the material.- We are interested in the path of the flow of material up to the point of melting or vaporizing. This is of particular interest in the study of tektites. To obtain the flow lines, we make an

approximate quasi-steady state analysis.

$$dx = \bar{\bar{u}}_x \, dt$$

$$dy = \bar{v} \, dt$$

$$dy/dx = \bar{v}/\bar{\bar{u}}_x$$

$$X_r(y,t) = \frac{x(y,t)}{x_{BF}} = e^{-\int_y^{y_{BF}} (\bar{\bar{u}}/\bar{v}) dy_1} \tag{68}$$

where x_{BF} is any selected small value of x at y_{BF} (where $\bar{\bar{u}} = 0$). Then $x = X_r x_{BF}$ gives $x(y)$ at time t for a flow line.

Aerodynamic deceleration.- For flight cases, we are interested in the aerodynamic deceleration of the body. We calculate the ratio of the aerodynamic force to the mass of the body to obtain the aerodynamic deceleration. We define a_{Dg} as the component of deceleration due to aerodynamic drag, normalized by the gravitational acceleration of the planet:

$$a_{Dg} = \frac{DV_\infty^2}{20 \left(\frac{M}{C_D A}\right) \left(\frac{g_p}{10^5}\right)} \tag{69}$$

The absolute value of the total normalized aerodynamic acceleration is

$$a_g = a_{Dg} \sqrt{1 + (L/D_r)^2} \tag{70}$$

Reradiation and apparent emissivity.- The terms for the fluxes of radiation at the front and back surfaces are given in equation (76). The rate of reradiation, from the front surface (absolute value) is F_{RS}. For opaque bodies,

$$F_{RS} = \epsilon_{FF} \sigma T_w^4 \tag{71}$$

The expression for the reradiation from the back surface of opaque bodies has a similar form. For opaque material, the surface emissivities, ϵ_{FF} and ϵ_{BF}, will be assigned values. For semitransparent material representation, the evaluation of ϵ_{FF} is as given in equation (45).

For transparent bodies, the situation is somewhat different. Here, we wish to calculate effective surface emissivities (which will vary with time). The flux of reradiation from the front surface is given by

$$F_{RS} = q_R - F(0,t) \tag{72}$$

Then we calculate:

$$\epsilon_{FF} = \frac{F_{RS}}{\sigma T_w^4} \tag{73}$$

Similarly, for the back face:

$$\epsilon_{BF} = \frac{F(y_{BF},t)}{\sigma T_{BF}^4} \tag{74}$$

The quantities, ϵ_{FF} and ϵ_{BF}, in equations (73) and (74) are the calculated effective surface emissivities for transparent material.

Energy Balance

Equation (1) is solved by numerical finite difference methods, and it is desirable to check the accuracy of solutions obtained. This is done by calculating a group of energy-integral terms listed below, summing them up, and determining the residual (error) in the sum. The magnitude of the energy integrals is also of interest, because it shows the disposition of the energies involved; this knowledge gives an insight into the processes of ablation.

We make the listing of the energy rate terms as follows:

The total convective heat-transfer rate into the material is

$$q_{con} = q_w + q_{BF} \tag{75}$$

The net radiative heating rate into the material is

$$q_{rad} = F(0,t) - F(y_{BF},t) + (1 - B_{16})[q_R - \epsilon_{FF}\sigma T_w^4 - \epsilon_{BF}\sigma(T_{BF}^4 - T_o^4)] \tag{76}$$

where

$B_{16} = 1$ for the transparent case

$B_{16} = 0$ for the opaque and semitransparent cases

and

$F \equiv 0$ for the opaque and semitransparent cases

The energy accounted for by the rate of vaporization (positive into the material) is

$$q_{vap} = \rho h_v \overline{v}_w \tag{77}$$

The energies put into the material are accounted for by terms that involve convection of the ablating material in the x and y directions and by a storage term. For the rate of increase of stored energy,

$$q_{stor} = \rho \frac{d}{dt} \int_o^{y_{BF}} \left[\int_{T_o}^{T(y_1)} c_p \, dT_2 \right] dy_1 \tag{78}$$

The x direction convection energy rate term (positive out) will be

$$q_{ucon} = 2\rho \int_o^{y_{BF}} \bar{\bar{u}} \left[\int_{T_o}^{T(y_1)} c_p \, dT_2 \right] dy_1 \tag{79}$$

The y direction convection energy rate term (positive out) is

$$q_{vcon} = -\rho \bar{v}_w \int_{T_o}^{T_w} c_p \, dT_1 \tag{80}$$

The error in the energy rate balance will be a residual term, q_{res}.

$$q_{res} = q_{con} + q_{rad} + q_{vap} - q_{stor} - q_{ucon} - q_{vcon} \tag{81}$$

The residual, q_{res}, shows the accuracy of the energy rate balance at any time, t.

The cumulative energy balance shows the total size of the various terms involved and the error accumulation. We compute the following integrals:

$$Q_{con} = \int_{t_i}^{t} q_{con} \, dt_1 \tag{82a}$$

$$Q_{rad} = \int_{t_i}^{t} q_{rad} \, dt_1 \tag{82b}$$

$$Q_{vap} = \int_{t_i}^{t} q_{vap} \, dt_1 \tag{82c}$$

$$Q_{stor} = \rho \int_o^{y_{BF}(t)} \left[\int_{T_o}^{T(y_1,t)} c_p \, dT_2 \right] dy_1 - \rho \int_o^{Y_{BF}(t_i)} \left[\int_{T_o}^{T(y_1,t_i)} c_p \, dT_2 \right] dy_1 \tag{82d}$$

$$Q_{ucon} = \int_{t_i}^{t} q_{ucon}\, dt_1 \tag{82e}$$

$$Q_{vcon} = \int_{t_i}^{t} q_{vcon}\, dt_1 \tag{82f}$$

So, for the accumulated residual we have:

$$Q_{res} = Q_{con} + Q_{rad} + Q_{vap} - Q_{stor} - Q_{ucon} - Q_{vcon} \tag{83}$$

METHOD OF THE NUMERICAL PROGRAM

Representations of Physical Properties

Most of the equations in the previous section contain (at least implicitly) quantities representing physical properties of the ablating material or external gas. The density of the ablating material, ρ, is assumed to be constant, but the other pertinent physical properties are considered to be temperature dependent. The temperature dependence of the physical properties has been left unspecified; however, to obtain numerical solutions, it will be specified by formulas with constants that can be arbitrarily chosen and read into the computing program. The representations used are:

Equilibrium vapor pressure of ablating material, atm

$$p_{ve} = e^{-\frac{B_2}{T_w} + B_3} \tag{84}$$

Viscosity of ablating material, poises

$$\mu = e^{\frac{B_4}{T - B_{14}} - B^5} \tag{85}$$

Specific heat of ablating material, cal/g ^{o}K

$$c = B_6 + E_1 T - \frac{B_7}{T^2} \tag{86}$$

Thermal conductivity of ablating material, cal/cm sec ^{o}K

$$K = B_9 + \frac{E_2}{T} + E_{20} T^3 \tag{87}$$

Average specific heat of external gas, cal/g ^{o}K (see eq. (14))

$$\overline{c}_p = E_{10} + E_3 T_w \tag{88}$$

Transformation of Coordinates and Finite Differencing

As described in the ANALYSIS AND METHOD OF SOLUTION section, the procedure in solving the system of equations presented is to make, in effect, all equations auxiliary to equation (1) which is solved with its appropriate boundary conditions as given in equations (46) and (47) or (51). Equation (1), a partial differential equation, is solved by a finite difference scheme; some complications are produced by the decrease of length with time between the front and back surfaces due to front surface recession. In this work, it was elected to keep the number of grid points constant, so the distance between grid points was allowed to shrink with decreasing length of the ablator. This was accomplished by the following transformation of independent variables from t, y to s, η, where

$$s = t \tag{89}$$

$$\eta = \frac{yL}{L - \chi(t)} \tag{90}$$

Then,

$$\frac{\partial}{\partial y} = \left[\frac{L}{L - \chi(s)}\right] \frac{\partial}{\partial \eta} \tag{91}$$

$$\frac{\partial}{\partial t} = \frac{\partial}{\partial s} + \left[\frac{(d\chi/ds)\eta}{L - \chi(s)}\right] \frac{\partial}{\partial \eta} \tag{92}$$

This transformation alters somewhat the form of equation (1) and the other equations as actually put into the numerical computing program.

Equation (1) is solved numerically by an explicit (forward difference) scheme. In finite difference form, the partial derivatives of the temperature, T, are represented as:

$$\left(\frac{\partial T}{\partial s}\right)_{m,n} = \frac{T_{m,n+1} - T_{m,n}}{\Delta s} \tag{93}$$

$$\left(\frac{\partial T}{\partial \eta}\right)_{m,n} = \frac{T_{m+1,n} - T_{m-1,n}}{2\Delta\eta} \tag{94}$$

$$\left(\frac{\partial^2 T}{\partial \eta^2}\right)_{m,n} = \frac{T_{m+1,n} - 2T_{m,n} + T_{m-1,n}}{(\Delta\eta)^2} \tag{95}$$

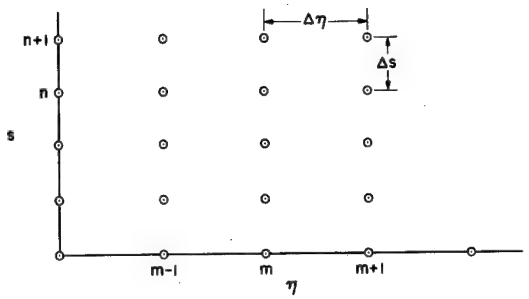

Sketch (b)

where m - 1, m, m + 1 are grid point numbers on the η (depth) scale and n, n + 1 are numbers on the s (time) scale as shown in sketch (b). Finite increments of s and η are indicated by the Δ symbol.

Stability and Accuracy of the Finite Difference Equation

In solving a parabolic partial differential equation by a forward difference scheme, there is always a stability requirement to be met. For the finite differencing of the transformed version of equation (1), the stability requirement turns out to be:

$$Z = \left[\frac{\Delta s}{(\Delta\eta)^2}\right]\left[\frac{L}{L - \chi(s)}\right]^2\left(\frac{K}{\rho c}\right) = \left[\frac{\Delta t}{(\Delta y)^2}\right]\left(\frac{K}{\rho c}\right) \leq \frac{1}{2} \qquad (96)$$

The stability parameter, Z, is printed out by the computing program for each grid point at each time printed. The increments of $\Delta\eta$ remain constant with time, but the increments of Δy decrease with time, as indicated by equation (90), until ablation is concluded. Thus, Z tends to increase somewhat while ablation is proceeding, and this must be considered in selecting initial increments. Since Z should not exceed 1/2, it is not possible to use the computing program to calculate to the point of complete extinction of an ablating material. When the present numerical program is used for transparent material, the storage limitation requires that the initial value of the ratio of length (depth) to the smallest $\Delta\eta$ be ≤ 1665 (see spacing sketch in appendix D).

A gross check on the accuracy of numerical solutions obtained is provided by the running energy balance and the cumulative energy balance (see ANALYSIS AND METHOD OF SOLUTION section). An additional check, standard in numerical work, can be made by varying Δs and $\Delta\eta$ and noting the resultant variations produced in the numerical solutions. This check, in effect, determines the adequacy of representing the derivatives by difference quotients with the finite increments as chosen (eqs. (93), (94), and (95)).

Boundary Conditions for Transparent Material

It was noted in the ANALYSIS AND METHOD OF SOLUTION section that the computing program can be arranged to modify the surface energy balance equations (46) and (47) for the transparent case. Equations (46) and (47) are rigorous as written, but they require a fine spacing of grid points, and therefore small time increments for stability. Particularly near the front

face, the derivative of the radiation flux, g, can change by orders of magnitude in a short distance. With a "normal" spacing of grid points, the fine structure of the variation of F and g are not well represented, and this can result in energy balances that are not accurate (large residuals). In the computing program, the front surface energy balance that we actually use for the transparent case ($B_{16} = 1$) is:

$$-\left(K\frac{\partial T}{\partial y}\right)_w = \rho h_v \bar{v}_w + q_w + E_{36}(F_w - F_{1/2}) \tag{97}$$

where $F_{1/2}$ is the radiation flux midway between the front surface and the first interior finite-differenced grid point (point number 1 + K2 in FORTRAN terminology; see spacing sketch in appendix D). For the back surface energy balance,

$$\left(K\frac{\partial T}{\partial y}\right)_{BF} = q_{BF} - E_{37}(F_{BF} - F_{BF-1/2}) \tag{98}$$

where $F_{BF-1/2}$ is the radiation flux midway between the back surface grid point and the nearest interior grid point. The quantities, E_{36} and E_{37}, are constants read into the program and will have values ≥ 0 and ≤ 1. When $E_{36} = E_{37} = 0$, we recover equations (46) and (47) exactly. E_{36} and E_{37} can be adjusted to give optimum energy balances; very good energy balances have been obtained with $E_{36} = E_{37} = 1$.

ILLUSTRATIVE EXAMPLES

Examples shown below illustrate the use of the numerical computing program as applied to several types of ablation. Calculated and measured results are compared for all examples except the last one, which is a Martian entry. The disposition of energies for typical examples given is summarized in table I.

Tektite Glass in a Wind Tunnel

Tektite glasses, ablated at high enthalpies in an arc-jet wind tunnel, furnish examples of ablators that both vaporize and melt. Typical comparisons between calculated and measured values of surface recession and surface brightness temperature are shown in figures 1 and 2. The measured points in figure 2 are actually a spread; measurements on other tektite glasses fell between these points. The agreement can be seen to be very good, which lends confidence that data for flights involving tektite glass can be successfully calculated (ref. 1). In both figures the calculations were made for a transparent glass and for a semitransparent glass, and there is little difference between the results of the two methods of computation. The glasses used in these examples ablate by melting more than by vaporizing because of the

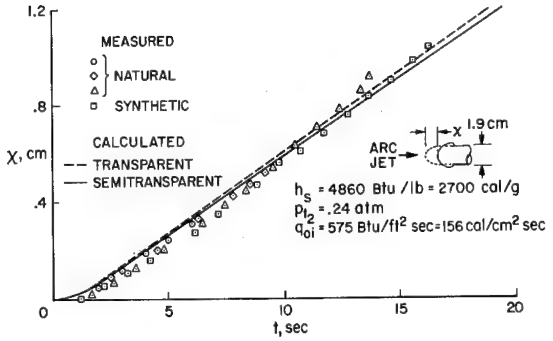

Figure 1.- Comparison of calculated and measured surface recession of tektite glass in a wind tunnel.

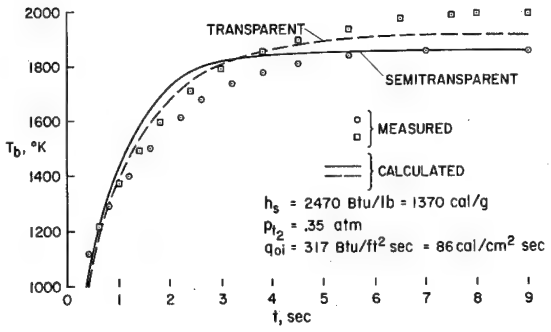

Figure 2.- Comparison of calculated and measured brightness temperature of tektite glass in a wind tunnel.

moderate enthalpy in the wind tunnel, the low viscosities, and low vapor pressures of the glasses. For the glasses in figure 1, about 1 percent of the ablation is due to vaporization, and for the glasses in figure 2, vaporization accounts for less than 1 percent. At higher enthalpies the relative amount of vaporization increases. Table I gives the disposition of energies calculated for the semitransparent glass of figure 1. Because of the small amount of vaporization, very little heat is blocked, and most of the incoming energy is accounted for by melting.

Tektite Entry Calculation

The results of calculating an entry for a typical opaque tektite are shown in figures 3 and 4. An entry speed of 11.0 km/sec and an entry angle of -30° were used for the calculations. These conditions correspond to a typical deduced trajectory for a Victoria australite (ref. 2, fig. 22). Figure 3 shows the calculated values of velocity, surface temperature, surface recession, and surface recession due to vaporization. The free-molecule and continuum regimes are also distinguished. Time zero is arbitrarily selected as "far out" before any appreciable aerodynamic heating has begun. This example illustrates the response of a material that vaporizes readily, with about 14 percent of the ablation due to vaporization and the rest to melting. As

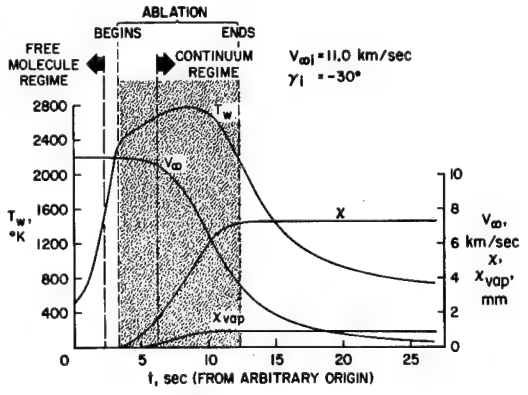

Figure 3.- Calculated variation of surface temperature, velocity, total ablation, and vaporized ablation for a Victoria australite entering the Earth's atmosphere; R_i = 0.816 cm.

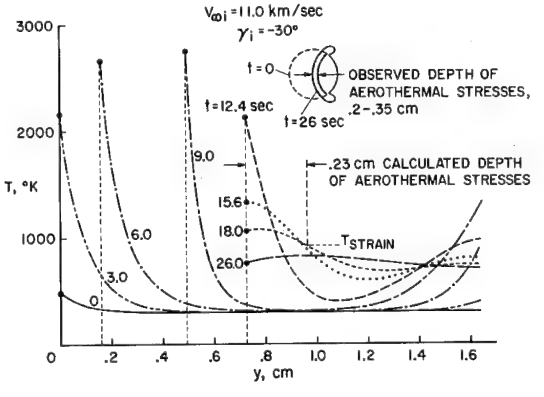

Figure 4.- Calculated temperature profiles for a Victoria australite entering Earth's atmosphere; R_i = 0.816 cm.

the tektite heats up, its surface begins to ablate at a temperature in excess of 2000 °K. The surface temperature and ablation rate reach a maximum and then fall off as the body slows down. The end of ablation occurs rather abruptly, and the remainder of the flight is that of a solid body being aerodynamically cooled. Measurements of the amount of ablation at the stagnation point (refs. 1 and 2) on recovered tektites yield values not greatly different from the 7.3 mm calculated for this example. The calculations indicate that for this flight, a negligible portion of the ablation occurred in the free-molecule regime. The portion of the ablation in the transitional regime was 24 percent, compared to the majority of ablation in the continuum regime (76 percent). For smaller tektites and shallow entry angles the percent of ablation in the free-molecule and transitional regimes will be greater; for large vehicles this portion of ablation is generally small.

In figure 4 are shown variations of the calculated temperature profiles and surface recession at selected values of time. This figure gives a fairly complete picture of the internal heating and eventual cooling of the body during its flight. The rise in the back temperatures is due to base heating. Measurements on recovered bodies by photoelasticity techniques show locked-in thermal stresses that vary from a depth of 0.2 to 0.35 cm, corresponding to the calculated depth of 0.23 cm (ref. 2). The post-flight observations of thermal stresses and deduced surface recession on recovered bodies are compatible with the calculated results. The energy disposition for the flight calculated is given in table I. The vaporization that occurs in this flight causes substantial heat blockage; the bulk of the energy is accounted for by heat blockage, heating and vaporizing, and heating and melt flow, these three quantities being of about the same order of magnitude.

Reentry Flight With Silica Glass Heat Shield

A calculation was made for a reentry flight of a nose-cone with an opaque silica glass heat shield. The vehicle and flight are described by Hidalgo and Kadanoff in reference 20. For this trajectory and this heat-shield material about 14 percent of the ablation was due to vaporization which is comparable to the tektite entry case previously discussed. The recovered reentry vehicle allowed the amount of ablation, X, at the stagnation point to be determined. The physical-property inputs in this case correspond to opaque silica (ref. 20), but both the transparent and the semitransparent options of the computing program were run with the results

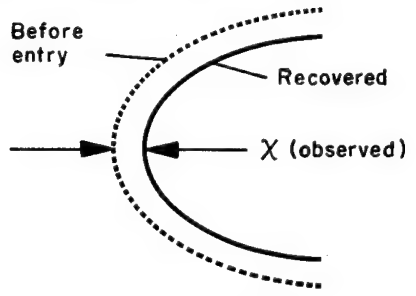

Sketch (c)

$$\frac{X(\text{transparent})}{X(\text{observed})} = 1.11 \qquad \frac{X(\text{semitransparent})}{X(\text{observed})} = 1.15$$

The corresponding ratio as calculated by Hidalgo and Kadanoff using their quasi-steady ablation analysis was about 1.10 and by Chapman and Larson (ref. 1), using an integral method of calculation, 0.92. This illustrates that the amount of ablation on simple materials such as glass can be computed to the order of 10- to 15-percent accuracy by several methods, including two of the options of the present computing program. In view of the inevitable angle-of-attack variations in flight, which cause the stagnation point of maximum heating to wander somewhat over the nose and thus reduce somewhat the maximum recession, the observed difference between calculated and measured ablation is in the expected direction. The energy disposition for both the transparent and semitransparent calculations is shown in table I. It is of interest that the two calculations yield energy proportions that are nearly the same, although the internal temperature distributions are different because of radiative transmission in the transparent case. In both cases the total ablation is moderate, so that the actual amount of vaporization is moderate and the heat blockage term is relatively small.

Teflon Model in an Arc-Jet Wind Tunnel

Under normal ablative conditions, tetrafluoroethylene polymer (Teflon) undergoes a surface depolymerization and vaporization of the monomer at a surface temperature of approximately 760 °K. There is no one specific temperature at which the reaction occurs, but a sharply rising reaction rate with temperature in this neighborhood essentially controls the surface temperature of an ablating model (refs. 21, 22). Under these conditions, the viscosity of Teflon remains high, so the process can be said to resemble a sublimation (with the reaction rate determined by an Arrhenius type rate equation). In performing the calculations for Teflon ablation, it was assumed that any energy involved in possible chemical reactions between the Teflon vapor and the external gases could be neglected.

Comparisons between calculated and experimentally measured surface recession for Teflon are shown in figure 5. The experiments by G. Lee and R. Sundell (ref. 23) were performed in an arc-jet wind tunnel for four values of enthalpy. It is seen that the agreement obtained is quite good, with the possible exception of the 700 Btu/lb total enthalpy case. It is thought that the generally satisfactory agreement shown in the figure indicates the validity of the method calculation and also that the physical properties of the substance have been adequately represented. The front face mass loss rate was essentially reaction rate controlled for the four cases shown in the figure.

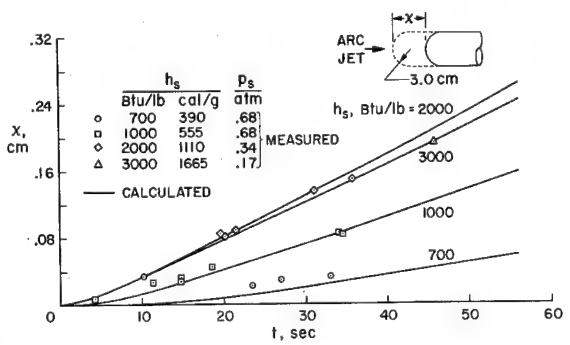

Figure 5.- Comparison of calculated and measured surface recession of Teflon in wind tunnel.

The disposition of the calculated energies for the 2000 Btu/lb total enthalpy case is shown in table I. The heat blockage term is fairly large

because all the ablated material leaves in the vapor state. The largest term is the energy for heating, depolymerizing, and vaporizing.

Teflon Heat Shield in a Mars Entry

The calculations for this example illustrate the application of the computing program to an entry with a proposed Mars probe (ref. 24). A spherical capsule of 61.0-cm diameter has been assumed, with a 1-cm thick Teflon heat shield, entering the Martian atmosphere in an oriented attitude. Four hypothetical atmospheres were assumed as tabulated below.

Composition (vol.)	Scale height, km
100% N_2	7.8
91% N_2, 9% CO_2	7.8
100% N_2	20.0
91% N_2, 9% CO_2	20.0

Subsequent to making these calculations, data obtained from the 1965 Mariner occultation experiment have indicated that the scale height of the Martian atmosphere is about 9 km (ref. 25). The assumed atmospheres with the 7.8 km scale heights thus appear to be the more realistic ones. Calculations were made for an entry velocity of 7.92 km/sec and for two entry angles, -90° and -20°. An M/C_DA for continuum flow of 3.91 g/cm^2 was assumed for the vehicle, and M/A was held constant while the C_D varied through the transition from the free-molecule to the continuum regimes.

The -90° entries have the greater peak heating rates, but the -20° entries absorb more total heat and are the more critical from a heat-shield standpoint. The heat-shield responses are compared using calculated values of the stagnation-point recession as tabulated below.

Atmosphere	Entry angle, deg	Total stagnation point recession, cm
N_2 small-scale height	-90	0.098
N_2 large-scale height	-90	.159
N_2-CO_2 small-scale height	-90	.121
N_2-CO_2 large-scale height	-90	.179
N_2-CO_2 small-scale height	-20	.196
N_2-CO_2 large-scale height	-20	.341

Of the -90° entries in the table, the most severe environment would be the mixed atmosphere and the large-scale height (although the small-scale height appears to be more realistic). For a given scale height, the mixed atmosphere gives somewhat more ablation than the nitrogen atmosphere because there is more radiation from the carbon dioxide (ref. 17). The time of exposure to heating is roughly proportional to scale height for two otherwise similar trajectories, and the total heat absorbed is approximately proportional to the square root of exposure time (and therefore scale height). This approximate relationship between scale height and total recession for a given atmospheric

composition can be deduced from the table. The strong dependence of the heat-shield response on any uncertainty of knowledge of atmospheric scale height is of interest, since this trend will presumably apply to any heat-shield material and any planet.

The disposition of energy for the -20° entry with the mixed atmosphere and short-scale height is shown in table I. As with the wind-tunnel results for Teflon, the two large energy terms are the heat blockage term and the term that accounts for heating, depolymerizing, and vaporizing. In the environment of the -20° Martian entry, the considerable amount of ablation of material to the vapor state accounts for the very large heat blockage term.

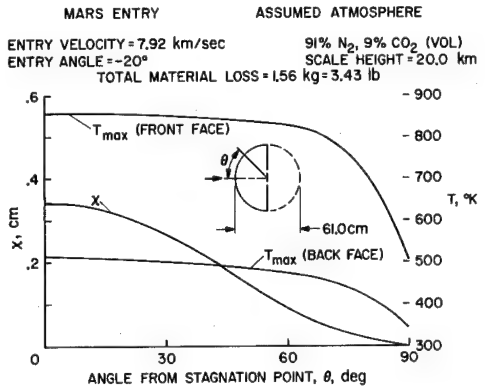

Figure 6.- Approximate calculation of response of a Teflon heat shield in a Mars entry.

As an illustration, the analysis has also been used in an approximate manner to calculate the quantities of interest around the front hemisphere of the spherical capsule for the -20° entry in the mixed atmosphere with the (probably overly severe) large scale height. The results are summarized in figure 6 which shows the variation of total recession and front and back face maximum temperatures around the hemispheric heat shield as well as the total mass loss for this hypothetical case. These results illustrate how variable material thickness may be used in heat-shield design.

TABLE I.- TYPICAL ENERGY BALANCES (percentages)

	Tektite glass (semitransparent) wind tunnel (fig. 1)	Tektite Earth entry (opaque) (figs. 3,4)	Silica glass heat-shield Earth entry (transparent)	Silica glass heat-shield Earth entry (semitransparent)	Teflon wind tunnel (fig. 5) h_s=2000 Btu/lb p_s=0.34 atm	Teflon Mars entry γ_i=-20° $V_{\infty i}$=7.92 km/sec
Convection in (hot wall)	100.0	100.0	100.0	100.0	100.0	100.0
Heat blocked	2.9	31.9	11.4	11.5	35.4	71.9
(Net convection in)	(97.1)	(68.1)	(88.6)	(88.5)	(64.6)	(28.1)
Net radiation in	-13.3	-10.8	-28.4	-27.6	-4.8	2.4
Heating and vaporizing	5.2	24.9	21.5	21.2	50.1	25.5
Heating and melting	69.1	27.2	28.6	31.6	0	0
Stored	4.6	6.3	10.4	6.9	9.9	5.1
Error	4.9	-1.1	-0.3	1.2	-0.2	-0.1

CONCLUDING REMARKS

A generalized analysis of stagnation-point ablation has been presented for solving a variety of problems involving melting and vaporizing, subliming, or surface chemical reactions. The flexibility of the analysis has been demonstrated through the presentation of several varied illustrative examples. In general, it is expected that accuracy of answers obtained will depend largely on the degree of knowledge of the physical, chemical, and thermodynamic properties of the ablating material, as these are necessary inputs for the computing program. The procedure of relating calculations for a given material to experiment wherever possible lends confidence to calculations for the same material exposed to other conditions which cannot be verified by observation.

Ames Research Center
National Aeronautics and Space Administration
Moffett Field, Calif., July 22, 1966
129-03-12-01-00

APPENDIX A

PRINCIPAL NOMENCLATURE

In performing computing machine calculations, some purely FORTRAN quantities are used, particularly among input data, which have no counterpart among the symbols listed below. These quantities are in appendix D, wherein all FORTRAN quantities are listed.

a	y direction body force per unit mass, cm/sec^2 (acceleration in flight)
a_{Dg}	component of deceleration due to aerodynamic drag normalized by gravitational acceleration of planet, dimensionless (eq. (69))
a_g	absolute value of aerodynamic acceleration normalized by gravitational acceleration of planet, dimensionless (eq. (70))
A	frontal area, cm^2
A_{cq}, A_{cv}, A_{cm}	free-molecule accommodation coefficients for heat transfer, mass loss, x momentum (for surface shear), respectively, dimensionless
A_{cv}'	corrected mass-loss accommodation coefficient (eq. (39c)), dimensionless
A_1	constant, defined by equation (27)
A_2	constant, defined by equation (11)
A_3	constant, defined by equation (32a)
A_4	constant, defined by equation (15)
A_{2D}	melt-off parameter, defined by equation (65), dimensionless
b	Sutherland constant, ^oK (eq. (C38))
B	Arrhenius frequency factor, cm/sec (eq. (39e))
B_2	constant in vapor pressure (eq. (84))
B_3	constant in vapor pressure (eq. (84))
B_4	constant in viscosity (eq. (85))
B_5	constant in viscosity (eq. (85))

B_6	constant in specific heat (eq. (86))
B_7	constant in specific heat (eq. (86))
B_9	constant in thermal conductivity (eq. (87))
B_{11}	constant in convective heat blockage factor (eqs. (28), (30)) (See discussion following eq. (C7).)
B_{14}	constant in viscosity (eq. (85))
B_{16}	constant; B_{16} = 1.0 for transparent case; B_{16} = 0 for opaque and semitransparent cases (eqs. (46), (47), (51))
c	specific heat of body material, cal/g ^{o}K
$\bar{c}$	heat capacity per unit area of backing material, cal/cm^2 ^{o}K (eq. (51))
c_p	specific heat of a gas at constant pressure, cal/g ^{o}K
$\bar{c}_p$	average specific heat, external gas, cal/g ^{o}K; defined by equation (14)
C_D, C_{DC}, C_{DFM}	drag coefficient, continuum drag coefficient, free-molecule drag coefficient, respectively, dimensionless
C_1	constant in nose radius (eq. (60))
C_2	constant in nose radius (eq. (60))
C_3	constant in M/A (eq. (56))
C_4	constant in M/A (eq. (56))
C_6	constant, vorticity correction in equation (15)
D	free-stream density, g/m^3
e_{al}	allowable error in T_w (selected), ^{o}K; allowable disagreement between T_w obtained from equations (1) and (46)
e_{rr}	error in T_w after last iteration, ^{o}K; will be $< e_{al}$
E_T	Arrhenius activation temperature, ^{o}K (eq. (39e))
$E_2(z)$	exponential integral (second degree), defined in equation (43)
E_1	constant in specific heat (eq. (86))
E_2	constant in thermal conducitivity (eq. (87))

E_3 constant in average specific heat (eq. (88))

E_4 constant in gas-cap radiation (eq. (44))

E_5 constant in gas-cap radiation (eq. (44))

E_6 constant in gas-cap radiation (eq. (44))

E_7 constant to account for shift of vaporization equilibrium (eq. (26))

E_8 constant in expression for shear blowing factor (eq. (34))

E_9 constant, defined by equation (58)

E_{10} constant in average specific heat (eq. (88))

E_{11} constant in expression for ρ_{21} (eq. (61))

E_{12} constant in expression for ρ_{21} (eq. (61))

E_{13} constant, defined by equation (50)

E_{14} constant depending on body shape and flight conditions in drag bridging (eq. (57)); see also equation (C46)

E_{15} constant accounting for body force in wind tunnel expression for ρ'' (eq. (10a))

E_{16} constant used in tumbling correction (eq. (12))

E_{17} constant in nose radius (eq. (60))

E_{18} constant in M/A (eq. (56))

E_{19} constant, defined by equation (49) as the ratio of turbulent to laminar base heating

E_{20} constant in thermal conductivity (eq. (87))

E_{33} constant used in expression for front face emissivity for semi-transparent body (eq. (45))

E_{35} constant, asymptotic value of ψ (eq. (28)) (See discussion following eq. (C7).)

E_{36}, E_{37} constants used in equations (97) and (98) to modify surface energy balances for the transparent case

E_{38} average ambient enthalpy for flight case, km^2/sec^2 (eq. (55))

f_μ ratio of actual viscosity to undissociated (Sutherland) value, dimensionless

F radiation flux, cal/cm^2 sec (eq. (41))

F_{RS} reradiation rate from front surface, cal/cm^2 sec (eqs. (71), (72))

$F_{1/2}$ radiation flux midway between front surface and first interior finite-differenced grig point, point number 1 + k2 in FORTRAN terminology; see Spacing Sketch in appendix D; cal/cm^2 sec (eq. (97))

$F_{BF-1/2}$ radiation flux midway between back surface grid point and nearest interior grid point, cal/cm^2 sec (eq. (98))

$\overline{F}$ ratio of surface recession rate due to vaporization to total surface recession rate, dimensionless (eq. (66))

$\overline{F}_t$ ratio of surface recession due to vaporization to total surface recession, dimensionless (eq. (67))

g gradient of radiative flux, $\partial F/\partial y$, cal/cm^3 sec

g_p gravitational acceleration of planet, cm/sec^2 (eq. (53b))

h enthalpy, cal/g

h_s stagnation enthalpy, cal/g

h_v latent heat of vaporization, cal/g

h_∞ average ambient enthalpy for flight case, cal/g (eq. (55))

$\overline{h}$ h/h_s, dimensionless

$\overline{\overline{h}}$ $(1 - \overline{h})/(1 - \overline{h}_w)$, dimensionless

K thermal conductivity, cal/cm sec ^oK

K_λ mean free path constant, moles (eq. (C40))

K_σ Reynolds analogy factor (eq. (31)), dimensionless

$\overline{K}$ fractional time center point is exposed to stagnation conditions, dimensionless (eq. (12))

$\overline{K}_{tu}$ correction factor for heat transfer and other quantities due to oscillation in flight, dimensionless (eq. (12))

L initial depth of material, cm

Le Lewis number, dimensionless

L/D_r	lift/drag ratio, dimensionless
m	molecular weight
$\dot{\bar{m}}$	mass loss rate, g/cm^2 sec
M	mass of body, g; also grid point number in finite difference computation
M_∞	free-stream Mach number, dimensionless
$\bar{M}$	m_e/m_v, dimensionless (eq. (29))
n	index of refraction, dimensionless; also exponent in equation (30)
p	pressure, $dynes/cm^2$ or atm, as specified
p_{t_2}	pressure downstream of normal shock, atm
p_v	actual vapor pressure, atm
p_{ve}	equilibrium vapor pressure, atm
p_{vm}	modified equilibrium vapor pressure, atm (eq. (26))
P	ratio of pressure of external gas to modified equilibrium vapor pressure of ablated vapor, dimensionless (eq. (26))
ρ''	negative of second derivative with respect to x of external pressure with a correction for body force, $dynes/cm^4$; defined in equation (8); evaluated in equation (10)
q	heat-transfer rate, cal/cm^2 sec; also dynamic pressure, $dynes/cm^2$
q_{oc}	surface convective (continuum) heat-transfer rate with no blowing, cal/cm^2 sec (eq. (15))
q_{FM}	surface convective (free molecule) heat-transfer rate, cal/cm^2 sec (eq. (17))
q_{oo}	surface convective heat-transfer rate with no blowing, bridged between q_{oc} and q_{FM}, cal/cm^2 sec (eq. (20))
q_o	q_{oo} corrected for tumbling or oscillation, cal/cm^2 sec (eq. (21))
q_{oc} $_{vort=o}$	q_{oc} without vorticity, cal/cm^2 sec; $C_\epsilon = 0$ in equation (15)
q_R	gas-cap radiation rate, cal/cm^2 sec (eq. (44))

$q_{\psi c}$ surface convective (continuum) heat-transfer rate with blowing, cal/cm^2 sec (eq. (16))

$q_{\psi w}$ surface convective heat-transfer rate (all regimes), bridged between $q_{\psi c}$ and q_{FM}, cal/cm^2 sec (eq. (18) or (22b))

q_w $q_{\psi w}$ corrected for tumbling or oscillation, cal/cm^2 sec (eq. (19) or (23))

q_{wRi} initial combined convective and radiative heating rate, cal/cm^2 sec (eq. (B3a))

Energy transfer rates listed below pertain to an energy balance, and, where applicable, are combined rates for front and back surfaces.

q_{con} total convective heat-transfer rate into material, cal/cm^2 sec (eq. (75))

q_{rad} net radiative heating rate into material, cal/cm^2 sec (eq. (76))

q_{vap} energy rate due to vaporization (positive if energy is released into the material), cal/cm^2 sec (eq. (77))

q_{stor} rate of increase of stored energy in the material, cal/cm^2 sec (eq. (78))

q_{ucon} x direction convection energy rate of the material (positive out), cal/cm^2 sec (eq. (79))

q_{vcon} y direction convection energy rate of the material (positive out), cal/cm^2 sec (eq. (80))

q_{res} residual in energy rate balance, cal/cm^2 sec (eq. (81))

$Q_{con}, Q_{rad}, Q_{vap}, Q_{stor}, Q_{ucon}, Q_{vcon}$ time integrals of corresponding q values, cal/cm^2 (eq. (82)); terms in total energy balance

Q_{res} residual in total energy balance, cal/cm^2 (eq. (83))

R nose radius, cm

R_b body radius, cm (eqs. (48), (50))

$R_{B/F}$ ratio of base to front-face laminar convective heating normalized by respective enthalpy potentials, for exposed back surface, dimensionless (eq. (48))

Re Reynolds number

R_{eff} effective coefficient of reflection for planar radiation, dimensionless (eq. (42))

Re_s Reynolds number based on enthalpy velocity (eq. (C20))

R_g universal gas constant, ergs/mole ^oK

R_p planet radius, km (eq. (53))

s transformed time coordinate, sec (eq. (89))

S collision cross-section area, cm^2 (eq. (C40))

S_h atmospheric scale height, km (eq. (54))

S_{h_i} initial scale height for entry into arbitrary atmosphere, km (eq. (B6)), and contained in equation (B10)

$S_{h_1}, S_{h_2}, S_{h_3}$ successive scale heights in arbitrary atmosphere, km:

$S_h = S_{h_1}$ when $\bar{\rho}_\infty \leq \bar{\rho}_{\infty_2}$;

$S_h = S_{h_2}$ when $\bar{\rho}_{\infty_2} < \bar{\rho}_\infty \leq \bar{\rho}_{\infty_3}$;

$S_h = S_{h_3}$ when $\bar{\rho}_\infty > \bar{\rho}_{\infty_3}$

t time, sec

t_i initial time, sec; time at which front face temperature, T_w, arrives at assumed T_{wi} for wind tunnel cases (eq. (B4))

T temperature, ^oK

T_b brightness temperature (emissivity unity), ^oK

T_o reference temperature, ^oK

$T_{\Delta\mu}$ viscosity thickness temperature, ^oK; temperature at which $\mu = e.\mu_w$ (at depth $\Delta\mu$)

u horizontal component of trajectory velocity, km/sec

u_e x direction velocity of external gas at edge of boundary layer, km/sec (eq. (11))

$\bar{u}$ velocity of material in x direction, cm/sec

$\bar{u}_e$ $u_e.10^5$, cm/sec

$\bar{\bar{u}}$ $\left(\frac{\partial \bar{u}}{\partial x}\right)_{x=o}$, sec^{-1}

u^*	$\bar{u}/\bar{u}_e$, dimensionless (eq. (C21))
v	vertical component of trajectory velocity (positive upward), km/sec
$\bar{v}$	velocity of material in y direction, cm/sec
$\bar{v}_{sr}$	surface recession rate, cm/sec (eq. (6a))
V	enthalpy velocity, km/sec; defined as $V^2 = 0.00836\ h_s$ (eq. (13))
V_∞	free-stream (trajectory) velocity, km/sec (eq. (52a))
x	longitudinal coordinate along meridian, cm
X_r	flow line ratio, dimensionless; defined by equation (68)
y	transverse coordinate normal to surface (inward), cm
Y	boundary-layer transverse coordinate, cm; appendix C
Z	stability parameter for finite differencing, dimensionless; (eq. (96)); must be $\leq 1/2$
α	absorption coefficient, internal radiation, cm^{-1} (eq. (41))
α_2	absorption coefficient, gas-cap radiation, cm^{-1} (eq. (41))
γ	trajectory angle, deg, positive above horizontal (eq. (52b))
δ	increment (appendix C)
δX	mass fraction, dimensionless (eq. (C10))
δ^*	displacement thickness, cm
Δ	thermal thickness, cm (eq. (63)); also increment e.g., Δh = enthalpy potential, cal/g
$\Delta_D, \Delta_q, \Delta_T$	unspecified characteristic boundary-layer thicknesses, cm (appendix C)
Δ_μ	viscosity thickness, cm; depth at which $\mu = e.\mu_w$
ϵ	surface emissivity, opaque or semitransparent; effective emissivity, transparent (eqs. (73), (74)); dimensionless
η	transformed y coordinate, cm (eq. (90)); also dummy variable
λ	mean free path, cm
μ	viscosity, poise

ρ	density of ablating material (constant), g/cm^3
ρ_{21}	density ratio across normal shock, dimensionless; for wind tunnel cases, assigned; for flight cases, equations (61) and (62)
$\overline{\rho}_\infty$	free-stream atmospheric density in Earth sea-level atmospheres, dimensionless, D/1226
$\overline{\rho}_{\infty_2}, \overline{\rho}_{\infty_3}$	values assigned to $\overline{\rho}_\infty$ at which changes of scale height in an arbitrary atmosphere occur; see S_{h_1}, S_{h_2}, S_{h_3}
σ	Stefan constant, 1.369×10^{-12} cal/cm^2 sec $^\circ K^4$; also Prandtl number, dimensionless
τ	shear, dynes/cm^2
φ	approximation of the ratio of stored energy to the stored energy associated with an exponential temperature profile, dimensionless (eq. (64))
χ	surface recession, cm
χ_{vap}	surface recession due to vaporization, cm; $\chi_{vap} = \overline{F}_t \chi$ (eq. (67))
χ_1	characteristic recession depth, cm, used in tumbling correction (eq. (12))
ψ	convective heat blockage factor, dimensionless (eqs. (16), (28))
$\overline{\psi}$	modified convective heat blockage factor, dimensionless (eqs. (22), (24))

Subscripts

a	actual
BF	back face
c	continuum
cha	change of wind tunnel conditions
d	diffusion
e	external gas or outer edge of boundary layer
eq	equilibrium
FF	front face

FM	free molecule
i	initial; this subscript can be combined with the others
max	maximum
o	no blowing
oc	no blowing, continuum
off	shut off of wind tunnel
r	reverse
ref	reference
s	stagnation (or settling chamber)
u	undissociated
v	vapor expelled
w	wall (front face)
wc	wall, continuum
wd	wall, diffusion
wFM	wall, free molecule
1	dummy variable
2	behind normal shock; also average condition between shock wave and body (appendix C)
∞	free stream

Superscript

'	x derivative

APPENDIX B

EQUATIONS FOR STARTING VALUES

To start the solution to equation (1), it is necessary to assign initial conditions. These will normally consist of a relatively low temperature profile which can exist before the onset of ablation. The particular selection of initial conditions is generally not critical as their influence damps out in a short time. The initial temperature profile that we assume is an exponential type.

$$T_i(y) = T_o + (T_{wi} - T_o)\left[e^{-y/\Delta_i} + R_{B/F}e^{-(y_{BF}-y)/\Delta_i}\right] \tag{B1}$$

If T_{wi} is selected near T_o, this profile amounts to a small perturbation on the constant T_o profile. We can take the y derivative of T_i at $y = 0$, equate it to the ratio of the heat flux (eq. (46)) to thermal conductivity at the wall, and solve for the initial thermal thickness, Δ_i.

$$\Delta_i = \frac{K_{wi}(T_{wi} - T_o)}{q_{wi} + (1 - B_{1\epsilon})q_{Ri}}\left(1 - R_{B/F}e^{-y_{BF}/\Delta_i}\right) \tag{B2a}$$

We use the more simple approximation:

$$\Delta_i \approx \frac{K_{wi}(T_{wi} - T_o)}{q_{wi} + (1 - B_{1\epsilon})q_{Ri}} \tag{B2b}$$

where $B_{1\epsilon} = 1$ for the transparent case and $B_{1\epsilon} = 0$ for the opaque and semitransparent cases. As described below in the section, Flight Cases, one option allows Δ_i to be assigned a value instead of obtaining it from equation (B2b). The initial convective and radiative heat fluxes needed in equation (B2b) are obtained differently for wind tunnel or flight as described below. In calculating q_{wi} and q_{Ri}, the initial free-stream density, D_i, is needed. For wind tunnel calculations, D_i will be known; for flight, D_i can be assigned or calculated as described below.

Ablation in a Wind Tunnel

The starting of a wind tunnel is visualized as a sudden step of a heat flux. We define a combined initial heat flux, q_{wRi}, as the sum of the initial convective and radiative fluxes.

$$q_{wRi} = q_{wi} + q_{Ri} \tag{B3a}$$

We assume that $\psi = 1$ and that the convective heat transfer is in the continuum regime (Q_{FMi} is not calculated). With $q_{wi} = q_{oci}$ we have:

$$q_{wRi} = q_{oci} + q_{Ri} \tag{B3b}$$

We evaluate q_{oci} from equation (15) and q_{Ri} from equation (44), with $\bar{K}_{tu} = 1$, using T_{wi} for T_w. If T_{wi} is small, q_{oci} and therefore q_{wRi} are approximately constant for a short period of time (eq. (15)). The classical conduction problem with a constant heat flux and constant properties (ref. 26, p. 56) can be used as an approximation for this case to determine the time at which the front face temperature arrives at the assumed T_{wi}. This turns out to be:

$$t_i = \frac{(T_{wi} - T_o)^2 \pi \rho c_{wi} K_{wi}}{4 q_{wRi}^2} \tag{B4}$$

One can set $T_{wi} \geq T_o$; the greater value is not necessary, but it gives the computing program a smooth start.

Flight With Arbitrary Initial Conditions

In starting the flight calculations, we will use an assigned initial velocity $V_{\infty i}$ and a flight path angle, γ_i, at (arbitrary) time, $t_i = 0$. The initial atmospheric density, D_i (equivalent to a starting altitude), can be assigned, as well as an initial thermal thickness, Δ_i. With an assumed T_{wi}, the initial profile is determined from equation (B1). Using this starting procedure, we do not require that Δ_i be consistent with the relationship given in equation (B2b). However, we calculate q_{wi}, q_{Ri}, and q_{wRi} as figures of interest as described below in the section, Initial Conditions for Entry Flight.

Initial Conditions for Entry Flight

An alternative starting procedure, valid for an entry flight, is to use an assigned $V_{\infty i}$ and γ_i and an assumed T_{wi}, and to calculate the entry into an exponential atmosphere [$D = Ce^{-(Alt/Sh_i)}$] which will raise the front face temperature to the assumed T_{wi}. The convective heating during this initial part of the entry will be considered to be of the free-molecule type (and we do not calculate q_{oci}). We can write (eq. (19)):

$$q_{wi} = q_{\psi wi} \bar{K}_{tu}$$

where

$$q_{\psi wi} = q_{FMi}$$

The evaluation of $\bar{K}_{tu}$ in equation (12) specializes to

$$\bar{K}_{tu} = \bar{K}$$

so we have

$$q_{wi} = \bar{K} q_{FMi}$$

We evaluate q_{FMi} from equation (17), and using equations (B3a) and (44), we have

$$q_{wRi} = \frac{\bar{K} A_{cq} D_i V_i}{0.0836} (V_i^2 - 0.00836\, \bar{c}_p T_{wi}) + \bar{K} E_4 R_i D_i^{E_5} V_i^{E_6} \qquad (B5)$$

where we use V_i as an approximation for $V_{\infty i}$.

The quantity q_{wRi} is the heating rate at time $t_i = 0$. Up to time $t_i = 0$, the heat flux will be approximately an exponential function of time, through the exponential variation of D. This is similar to a classical problem in heat conduction (ref. 26, p. 45) which yields an exponential temperature profile. In equation (B5) we can replace D_i by D as an exponential function of altitude; we can approximate the slightly varying enthalpy potential as a constant (the value in eq. (B5)); and we can integrate the heating flux over time from $t = -\infty$ to $t = t_i = 0$. We obtain, then, the total heat absorbed:

$$Q_{total} = \frac{S h_i \bar{K} A_{cq} D_i (V_i^2 - 0.00836\, \bar{c}_p T_{wi})}{0.0836\, |\sin \gamma_i|} + \frac{S h_i \bar{K} E_4 R_i D_i^{E_5} V_i^{E_6 - 1}}{E_5 |\sin \gamma_i|} \qquad (B6)$$

We can also approximate the total heat absorbed as

$$Q_{total} \approx \rho c_{wi} \int_0^{y_{BF}} (T - T_o)\, dy \qquad (B7)$$

When we substitute the profile equation (B1) into equation (B7), we obtain

$$Q_{total} \approx \rho c_{wi} (T_{wi} - T_o) \Delta_i (1 + R_{B/F}) \left(1 - e^{-y_{BF}/\Delta_i}\right) \qquad (B8a)$$

or, approximated further,

$$Q_{total} \approx \rho c_{wi} (T_{wi} - T_o) \Delta_i \qquad (B8b)$$

We substitute q_{wi} and q_{Ri} (the first and second terms, respectively, on the right side of eq. (B5)) into equation (B2b) for Δ_i, put this into equation (B8b), and have finally

$$Q_{total} \approx \frac{\rho c_{wi} K_{wi} (T_{wi} - T_o)^2}{\frac{\bar{K} A_{cq} D_i V_i}{0.0836} (V_i^2 - 0.00836\, \bar{c}_p T_{wi}) + \bar{K} E_4 R_i D_i^{E_5} V_i^{E_6}} \tag{B9}$$

We now eliminate Q_{total} from equations (B6) and (B9) and we obtain an equation of the form

$$\left(D_i + \frac{K_1}{E_5} D_i^{E_5}\right)\left(D_i + K_1 D_i^{E_5}\right) = K_2 \tag{B10}$$

where K_1 and K_2 are constants and D_i is the only unknown.

The procedure, then, for starting the entry calculations is as follows. We assume a T_{wi} and we know the scale height, S_{h_i}, far out in an atmosphere. We use equation (B10) to calculate D_i; we can then calculate q_{wi} and q_{Ri} as the first and second terms, respectively, on the right side of equation (B5). Finally, we obtain Δ_i from equation (B2b), and we put Δ_i into the profile equation (B1). We can see that the assumption of T_{wi} fixes the D_i, or, in effect, fixes the altitude at which we start time zero. For this case, $T_{wi} > T_o$ is necessary in order to have a finite starting altitude.

APPENDIX C

BRIDGING BETWEEN FREE-MOLECULE AND CONTINUUM REGIMES

For a number of applications or situations, it is known that the transitional regime between free-molecule and continuum flow must be considered. The bridging formulas used in this work for the transitional regime are presented without derivations, in the ANALYSIS AND METHOD OF SOLUTION section as equations (18), (20), (24), (37), (40), and (57). The derivations of these equations, based principally on a simple kinetic theory model, are given in this appendix. These bridging formulas replace previously used equations which were of purely empirical form (ref. 1).

Front Face Normal Velocity

For the front face normal velocity or mass loss rate, a bridging relationship is required between the free-molecule and continuum regimes. We will consider first the free-molecule or reaction rate-controlled regime, and we will distinguish between the evaporation or sublimation case and the chemical reaction case.

For the case involving evaporation or sublimation, we write the Langmuir equation (eq. (76) of ref. 27) for the mass loss rate into a vacuum as:

$$\dot{m}_{FM} = A_{cv} p_{ve} C_{dy} \sqrt{\frac{m_v}{2\pi R_g T_w}} \tag{C1}$$

where the constant, C_{dy}, is the pressure of a standard atmosphere in dynes/cm^2 so that p_{ve} is measured in atmospheres, m_v is the molecular weight in g, and R_g is the universal gas constant in erg/mole ^{o}K. Equation (C1) is based on the rate of molecules crossing a unit area, in this case impacting against a unit surface area, and the accommodation coefficient, A_{cv}, is the fraction of the molecules that stick to the surface and condense. At equilibrium the evaporation and condensation rates are equal so there is then no net evaporation rate. At a given temperature, the rate of surface impacts, and therefore the rate of condensation, is proportional to the actual vapor pressure above the surface, p_v. So we can write for the condensation rate:

$$\dot{m}_r = \frac{p_v}{p_{ve}} \dot{m}_{FM} \tag{C2}$$

and for the net rate of evaporation (or sublimation)

$$\dot{m} = \dot{m}_{FM} - \dot{m}_r \tag{C3a}$$

$$\dot{\bar{m}} = \dot{\bar{m}}_{FM}\left(1 - \frac{p_v}{p_{ve}}\right) \qquad (C3b)$$

If the equilibrium vapor pressure is shifted or modified by the presence of other gaseous materials in the boundary layer, then the largest actual vapor pressure at the surface, p_v, that can be reached is the modified equilibrium vapor pressure, p_{vm} (see eq. (26)), rather than p_{ve}. We accordingly modify equation (C3b) and use the approximate expression:

$$\dot{\bar{m}} = \dot{\bar{m}}_{FM}\left(1 - \frac{p_v}{p_{vm}}\right) \qquad (C3c)$$

For the chemical reaction case we rewrite the Arrhenius rate equation for a first order reaction (eq. (39e)) as

$$\dot{\bar{m}}_{FM} = \rho B e^{-E_T/T_w} \qquad (C4)$$

When the modified equilibrium vapor pressure, p_{vm}, exists above the surface, the net reaction rate is zero, or the reverse reaction rate equals the forward reaction rate. At a given temperature, the rate of impact of vapor molecules with the surface will again be proportional to the actual vapor pressure at the surface, p_v. We can assume that the reverse reaction rate, $\dot{\bar{m}}_r$, is proportional to the rate of surface impacts and therefore to the actual vapor pressure, p_v, and we again have equation (C3c) for the net reaction rate.

We now consider the continuum or diffusion controlled regime for the front face mass loss rate. The limiting value of the diffusion controlled front face normal velocity, $|\bar{v}_{wc}|$, is given in equation (38), and we define $\dot{\bar{m}}_d = \rho|\bar{v}_{wc}|$ (obtained by putting ρ on the left side of eq. (38)), as the limiting value or maximum mass diffusion rate. As noted in the discussion following equation (38), this evaluation is obtained using P and ψ which ultimately depend on the modified equilibrium vapor pressure at the surface, p_{vm}. As distinct from the theoretical or limiting value, $\dot{\bar{m}}_d$, we next consider the actual mass transfer rate by diffusion. The actual rate can be shown to be approximately proportional to the actual vapor pressure at the surface, p_v, by inserting actual, rather than limiting, evaluations of P and ψ into equation (38). In these actual evaluations, P will be based on p_v rather than p_{vm} and the ψ asymptote is assumed to be ≈ 0 with $B_{11} \approx 1$. We then obtain

$$\dot{\bar{m}} = \dot{\bar{m}}_d\left(\frac{p_v}{p_{vm}}\right) \qquad (C5a)$$

This is straightforward when $p_{vm} < p_{t_2}$. When $p_{vm} \geq p_{t_2}$, a modification is necessary because in equation (38) we have, in effect, given p_{vm} an upper limit of $0.999{,}999\ p_{t_2}$. In this case we have

$$\dot{m} = \dot{m}_d \left(\frac{p_v}{p_{t_2}}\right) = \left[\dot{m}_d \left(\frac{p_{vm}}{p_{t_2}}\right)\right] \left(\frac{p_v}{p_{vm}}\right) \tag{C5b}$$

Let

$$\dot{m}_d' = \dot{m}_d \left(\frac{p_{vm}}{p_{t_2}}\right) \tag{C6}$$

and we have equation (C5a) with $\dot{m}_d'$ replacing $\dot{m}_d$.

If a quasi-steady state is assumed, there is no accumulation or depletion of vapor in the boundary layer. Thus the actual mass loss rate calculated by the free-molecule (reaction-rate) method, and the actual mass loss rate calculated as a diffusion process must be the same; physically this means that the actual vapor pressure at the surface, p_v, must have a value such that $\dot{m}$ obtained from equations (C3c) and (C5) will be the same. We eliminate p_v/p_{vm} between equations (C3c) and (C5a) and obtain

$$\frac{1}{\dot{m}} = \frac{1}{\dot{m}_{FM}} + \frac{1}{\dot{m}_d} \tag{C7}$$

At high mass loss rates, one can surmise that diffusion control may merge into a hydrodynamic control with an interface between the two fluids. In this case, equation (38) may yield values of the "diffusion" rate that are too large at the high mass loss rates. Finite values of the "diffusion" rate will be obtained from equation (38) when the ψ asymptote $E_{35} = 0$, and $B_{11} = 1$. For the (somewhat unusual) situation when $p_{vm}/p_{t_2} > 0.8$, it is suggested that one use $E_{35} = 0$ and $B_{11} \approx 1$; this insures that $\dot{m}_d = \rho|\bar{v}_{wc}|$, as calculated using equation (38), does not become unrealistically large. For the condition with $p_{vm} \geq p_{t_2}$, we should actually replace $\dot{m}_d$ with $\dot{m}_d'$ in equation (C7). However, this situation will generally be one of rate control in which $\dot{m}_{FM}$ will be small relative to $\dot{m}_d$ (whose calculated value may be too large) and $\dot{m}_d'$ will be still larger. As an approximation for all conditions, we will accordingly, use equation (C7) with $\dot{m}_d$.

When we cancel out the constant density, ρ, from equation (C7), we have equation (40) for the front face normal velocity, $\bar{v}_w$. A somewhat similar line of reasoning for the evaporation case is in reference 28 although bridging equations are not presented. These bridging forms (eqs. (40) and (C7)) are considered to be valid approximations over the complete spectrum from rate control to diffusion control; the use of the bridging relationship automatically places control in the proper regime. Some verification of this bridging relationship is given in figure 5 by the comparisons between calculations and experiment for the ablation of Teflon in a wind tunnel. These examples are essentially reaction rate controlled, except for $h_s = 3000$ Btu/lb which is considered to be in the transitional regime.

To calculate heat transfer in the transitional regime, we require a bridging between the continuum and free-molecule heat transfer values given by equations (16) and (17). The bridged result is shown in equation (18). A very simple first-collision model is used in the analysis. A typical packet of free molecules is assumed to enter the boundary layer and make a first collision with molecules already there. The free molecules then become part of the continuum boundary layer with average energy equal to that of the boundary layer at the point of the collision. The energy given up by the free molecules on collision is assumed to be ultimately taken up by the wall (by successive collisions in the continuum boundary layer and impact with the wall), since there is no piling up of energy in a quasi-steady state boundary layer. (Some of the free molecules will make their first collision with the wall and give up energy directly.)

We use a normalized enthalpy, $\bar{h} = h/h_s$, and the coordinate system shown in sketch (d). We define an effective collision thickness, Δ_q, such that collisions occurring within Δ_q have an effect on wall heat transfer, while collisions occurring outside of Δ_q have a negligible effect on wall heat transfer; Δ_q is thus a kind of boundary layer thickness. We can rewrite equation (17) as

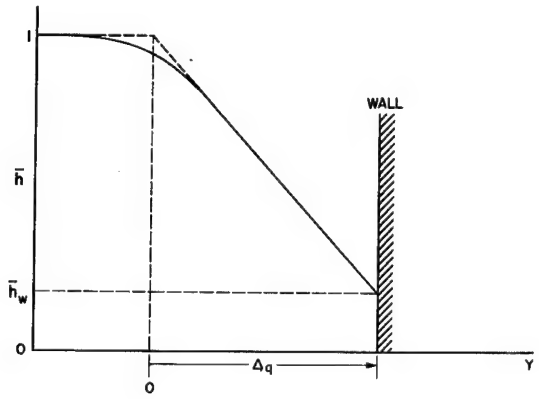

Sketch (d)

$$q_{FM} = K_1(DV_\infty)h_s(1 - \bar{h}_w) \qquad (C8)$$

where K_1 contains the conversion of units and the accommodation coefficient, A_{cq} (assumed to be approximately unity). Then, for a small packet of molecules entering the boundary layer and making its first collision, our assumed model allows us to write:

$$\delta q_{FM} = [h_s K_1(DV_\infty)]\delta X(1 - \bar{h}) \qquad (C9)$$

where δX is the mass fraction of molecules that make the first collision between Y and $Y + dY$ (or between $\bar{h}$ and $\bar{h} + d\bar{h}$) in the boundary layer; δq_{FM} is heat given up by the fraction δX. In using K_1 in equation (C9), we are assuming that the fraction of energy given up in the molecular collisions is the same as the fraction given up by collisions with the wall (approximately unity); this is thought to be within the framework of approximations being made in the derivation. The mass fraction, δX, is evaluated in terms of the mean free path, λ (ref. 29, eq. (103-7)).

$$\delta X = e^{-Y/\lambda}\,\frac{dY}{\lambda} \qquad (C10)$$

The mean free path, λ, is actually a function of Y since λ varies inversely with density in the boundary layer. We will consider λ to have some constant mean value in the boundary layer in order to perform an integration (below). This assumption appears to be within the framework of approximations being made. In accord with our quasi-steady-state assumption, we write

$$q_{\psi w} = \sum_{\text{all } \delta X} \delta q_{FM} \tag{C11}$$

and using equation (C9) we have

$$\frac{q_{\psi w}}{[h_s K_1 (DV_\infty)]} = \frac{\sum_{\text{all } \delta X} \delta q_{FM}}{[h_s K_1 (DV_\infty)]} = \sum_{\text{all } \delta X} \delta X (1 - \bar{h}) \tag{C12}$$

We insert δX from equation (C10) and have:

$$\frac{q_{\psi w}}{[h_s K_1 (DV_\infty)]} = \int_{\text{all } \delta X} (1 - \bar{h}) e^{-Y/\lambda} \frac{dY}{\lambda} \tag{C13}$$

We will use:

$$\bar{\bar{h}} = \frac{1 - \bar{h}}{1 - \bar{h}_w} = f\left(\frac{Y}{\Delta_q}\right) \tag{C14}$$

and we can write:

$$\frac{q_{\psi w}}{[h_s K_1 (DV_\infty)]} = (1 - \bar{h}_w) \left[\int_o^{\Delta_q} \bar{\bar{h}} e^{-Y/\lambda} \frac{dY}{\lambda} + e^{-\Delta_q/\lambda} \right] \tag{C15}$$

The last term in the bracket accounts for heat transfer from the molecules whose free path is greater than Δ_q (ref. 29, eq. (103-8)). Using equations (C8 and C14) we have finally

$$q_{\psi w} = q_{FM} \left[\int_o^{\Delta_q} f\left(\frac{Y}{\Delta_q}\right) e^{-Y/\lambda} \frac{dY}{\lambda} + e^{-\Delta_q/\lambda} \right] \tag{C16}$$

We will use the simplest form for $f(Y/\Delta_q)$ in equation (C14) (see sketch (d)).

$$\bar{\bar{h}} = f\left(\frac{Y}{\Delta_q}\right) = \frac{Y}{\Delta_q} \tag{C17}$$

We perform the integration in equation (C16) and obtain

$$q_{\psi w} = q_{FM}\left[\frac{\lambda}{\Delta_q}\left(1 - e^{-\Delta_q/\lambda}\right)\right] \tag{C18}$$

To consider a variation in the ratio, λ/Δ_q, we can visualize a change in ambient density, D. The mean free path, λ, varies as D^{-1}, and Δ_q (being a kind of boundary layer thickness) varies as $D^{-1/2}$, so the ratio, λ/Δ_q, varies as $D^{-1/2}$. In the free-molecule limit, λ/Δ_q becomes very large, and in the continuum limit, very small. When λ/Δ_q is large, $q_{\psi w}$ approaches q_{FM} in equation (C18), as it should. When λ/Δ_q is small, $q_{\psi w}$ must approach $q_{\psi c}$. Using equation (C18) we can write for small λ/Δ_q

$$q_{\psi w} = q_{\psi c} = \frac{\lambda}{\Delta_q} q_{FM} \tag{C19a}$$

$$\frac{\Delta_q}{\lambda} = \frac{q_{FM}}{q_{\psi c}} \tag{C19b}$$

The quantities, q_{FM} and $q_{\psi c}$, are calculated values for given (the same) conditions. Since the characteristic thickness, Δ_q, has not been specified, it can now be given the value that satisfies equation (C19b) for the conditions imposed. The mean free path, λ, has been considered to be some mean value in the boundary layer, and it can be assigned a convenient value, say λ_2, with Δ_q required to satisfy equation (C19b) with this λ. It can be shown that the form of equation (C19b) is a consistent relationship by making use of equations (5.5), (6.23), (6.25), (6.56) of reference 30, and relating λ to a characteristic thickness (displacement thickness, δ^*).

We substitute equation (C19b) into (C18) and we have equation (18) as the bridging equation for convection heat transfer.

$$q_{\psi w} = q_{\psi c}\left(1 - e^{-q_{FM}/q_{\psi c}}\right) \tag{18}$$

Equation (18) has the form of a monotonic function of $q_{FM}/q_{\psi c}$, and it has the correct free-molecule and continuum regime asymptotes. The derivation has been essentially performed from the free-molecule end, and the agreement with the continuum end has been forced. In the derivation, functional forms for $f(Y/\Delta_q)$ other than the simple one chosen (eq. (C17)) can be used. The result will be similarly behaved, but more complicated, bridging equations. It is possible that the more complicated equations that can be obtained may give better agreement with measured data for some specific types of heat transfer.

The alternate forms of the bridging relations (eqs. (20) to (24)) are obtained directly from equation (18) as outlined in the ANALYSIS AND METHOD OF

SOLUTION section. The alternate forms yield the quantities, q_{oo}, q_o, and $\bar{\psi}$ (which are mainly of conceptual interest).

Comparisons of calculated bridging with experiment are available for the case with no blowing. Experimental data, obtained from figure 5 of reference 31, are shown plotted in figure 7 and compared with calculated values of continuum heat transfer, free-molecule heat transfer, and the bridged heat transfer value obtained from equation (20). The data shown are stagnation-point heat-transfer measurements on a spherical body at nominal Mach numbers of 5.7 and 8 with stagnation temperatures of 2100° to 2300° R. The quantities, q_{oc} (eq. (15)), q_{FM} (eq. (17)), and q_{oo} (eq. (20)) are all normalized using the continuum heat-transfer rate with zero vorticity, q_{oc} . This normalizing factor is obtained from equation (15) with the vorticity correction dropped ($C_6 = 0$). The Reynolds number used as abscissa, Re_s, is based on the enthalpy velocity (eq. (13b)) and the stagnation gas properties, as originally used in reference 31.

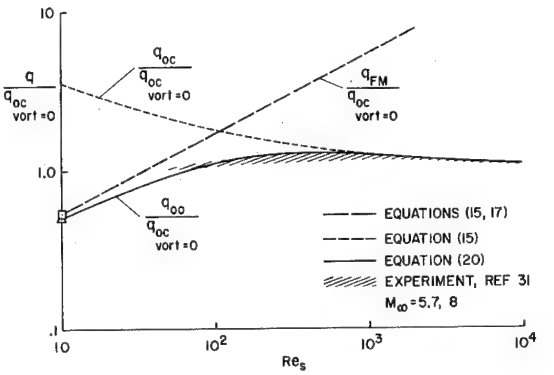

Figure 7.- Comparison of calculated convective heat transfer bridging with experiment for the case without blowing.

$$Re_s = \frac{V\rho_{21}DR}{10\mu_s} \qquad (C20)$$

In the experiments of reference 31, the Reynolds number was varied by mainly varying the free-stream density, D, and the nose radius, R. It is seen from the figure that the calculated bridging checks well with experiment.

Comparisons were also made (not shown here) with measured data from reference 32 for subsonic heat transfer from spheres. Equation (20) checks these data reasonably well.

It is concluded from the comparisons made that the bridging relation in equation (18) should be a useful approximation for the general case with blowing since equation (20) is simply a specialization (with the form unchanged) of equation (18), and equation (18) has the correct asymptotes for the general case. Experimental verification for the blowing case would be desirable.

Surface Shear

For the calculation of the (x derivative of) surface shear in the transitional regime, we bridge between equations (35) and (36) to obtain equation (37). The first collision model used is the same as that used for convective heat transfer, except that we are now concerned with the transfer of x momentum rather than energy.

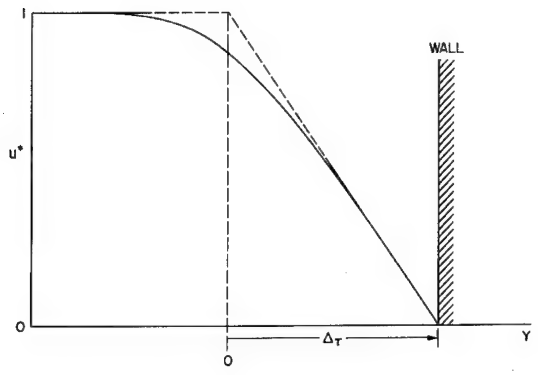

Sketch (e)

We use the coordinate system shown in sketch (e), and we introduce

$$u^* = \frac{(d\bar{u}/dx)_{x=o}}{(d\bar{u}_e/dx)_{x=o}} = \frac{\bar{u}}{\bar{u}_e} \qquad (C21)$$

We assume that collisions occurring within an effective collision thickness, Δ_T (a kind of boundary layer thickness), affect surface shear, while those occurring outside Δ_T have a negligible effect. Making use of equation (11), we rewrite equation (36) as

$$\tau'_{wFM} = K_4(DV_\infty)\left(\frac{d\bar{u}_e}{dx}\right)_{x=o} \qquad (C22)$$

where K_4 contains the conversion of units and the accommodation coefficient, A_{cm}, considered to be approximately unity. Using the same reasoning and analogous development as that used for convective heat transfer, we can write

$$\tau'_w = \sum_{\text{all } \delta X} K_4(DV_\infty)\delta X\left(\frac{d\bar{u}_e}{dx} - \frac{d\bar{u}}{dx}\right) \qquad (C23a)$$

$$\tau'_w = \tau'_{wFM} \sum_{\text{all } \delta X} \delta X(1 - u^*) \qquad (C23b)$$

We evaluate δX according to equation (C10) and obtain:

$$\tau'_w = \tau'_{wFM}\left[\int_o^{\Delta_T} (1 - u^*)e^{-Y/\lambda}\frac{dY}{\lambda} + e^{-\Delta_T/\lambda}\right] \qquad (C24)$$

We use (see sketch (e))

$$1 - u^* = f\left(\frac{Y}{\Delta_T}\right) \qquad (C25)$$

and have

$$\tau'_w = \tau'_{wFM}\left[\int_o^{\Delta_T} f\left(\frac{Y}{\Delta_T}\right)e^{-Y/\lambda}\frac{dY}{\lambda} + e^{-\Delta_T/\lambda}\right] \qquad (C26)$$

As was done with the convective heat transfer bridging, we evaluate $f(Y/\Delta_T)$ in the simplest way (see sketch (e)):

$$1 - u^* = f\left(\frac{Y}{\Delta_T}\right) = \frac{Y}{\Delta_T} \tag{C27}$$

The integration of equation (C26) then yields

$$\tau_w' = \tau_{wFM}' \left[\frac{\lambda}{\Delta_T}\left(1 - e^{\Delta_T/\lambda}\right)\right] \tag{C28}$$

The ratio, λ/Δ_T, becomes very large in the free-molecule limit and very small in the continuum limit in a manner similar to λ/Δ_q (as described above in the Convective Heat Transfer section). When λ/Δ_T is large, τ_w' in equation (C28) approaches τ_{wFM}' as it should. When λ/Δ_T is small, τ_w' must approach τ_{wc}'. From equation (C28) we get

$$\frac{\lambda}{\Delta_T} = \frac{\tau_{wc}'}{\tau_{wFM}'} \tag{C29}$$

Since the characteristic thickness, Δ_T, has not been specified, it can now be defined as having values that satisfy equation (C29). We are thus forcing our bridging relationship to have the correct continuum asymptote.

We can show directly that equation (C29) is a consistent relationship by making use of equations (5.6, 6.23, 6.25, 6.29, 6.30, 6.32, and 6.41) of reference 30. We can also show the consistency of equation (C29) by using the heat-transfer relations that we have. By combining equations (16), (17), (35), and (36) we obtain

$$\frac{\tau_{wc}'}{\tau_{wFM}'} = \left[\frac{A_3 A_{cq}\left(1 + \frac{E_8}{P}\psi\right)}{A_{cm}\sqrt{\rho_{21}}}\right]\left(\frac{q_{\psi c}}{q_{FM}}\right) \tag{C30}$$

Then, using equation (C19b), we have

$$\frac{\tau_{wc}'}{\tau_{wFM}'} = \left[\frac{A_3 A_{cq}\left(1 + \frac{E_8}{P}\psi\right)}{A_{cm}\sqrt{\rho_{21}}}\right]\left(\frac{\lambda}{\Delta_q}\right) \tag{C31}$$

This gives equation (C29) when

$$\Delta_T = \left[\frac{A_{cm}\sqrt{\rho_{21}}}{A_3 A_{cq}\left(1 + \frac{E_8}{P}\psi\right)} \right] \Delta_q \qquad (C32)$$

When we substitute equation (C29) into (C28), we have the bridging relation for the x gradient of surface shear.

$$\tau'_W = \tau'_{WC}\left(1 - e^{-\tau'_{WFM}/\tau'_{WC}}\right) \qquad (37)$$

If functional forms for $f(Y/\Delta_T)$ other than the simple one in equation (C27) are chosen for the derivation given above, the bridging equations will be more complicated than equation (37) but similarly behaved. It is possible that some of the more complicated forms may furnish more accurate bridgings for some specific shear situations.

Direct experimental verifications of equation (37) applied to the stagnation region with blowing have not been found. However, it is believed that this relationship is a reasonable and useful approximation for surface shear in the transitional regime. The expression is a monotonic function of τ'_{WFM}/τ'_{WC} and it has the correct free-molecule and continuum regime asymptotes.

Although equation (37) was derived for a stagnation region boundary layer, it is of possible interest to compare calculated results with subsonic flat plate shear measurements since these data are available. This comparison is shown in figure 8. The measured data are from figure 9(a) of reference 32. The agreement shown in figure 8 is thought to be surprisingly good.

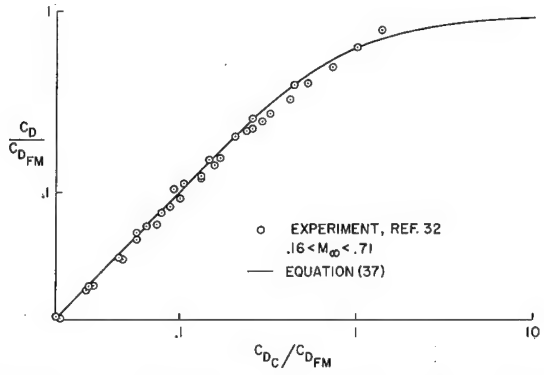

Figure 8.- Comparison of calculated skin friction bridging with measured skin friction for subsonic flat plate (without blowing).

An attempt was also made to compare calculated shear from equation (37) with measured shear in low speed Couette flow as reported in reference 33 (not shown); the agreement obtained was fair. An equation derived for Couette flow by the authors of reference 33 checks the data very closely; this illustrates that one should generally prefer a bridging equation derived for a specific situation if this be available.

Drag Bridging

For flight calculations, we use the trajectory equations (52) to (54), in which the quantity, M/C_DA, appears. The evaluations of C_D and M/C_DA are given in equations (57) and (59), respectively, equation (57) being the

bridging formula for C_D. A bridging relation for the drag coefficient is clearly necessary for entry flights since C_D must initially have a free-molecule evaluation, and, for many entries, the final value of C_D will be the continuum value.

To evaluate the drag bridging, we again make use of our first-collision model (in a treatment that amounts to a further approximation with the model). We again use an unspecified characteristic effective collision thickness, Δ_D, and assume that collisions outside of Δ_D have a negligible effect on drag. We assume, then, that the molecules that have a longer free path than Δ_D make their first effective collision with the body and contribute to free-molecule drag. The other molecules collide with each other within the depth, Δ_D; these molecules bathe the body in a continuum fluid and contribute to continuum drag. A more rigorous development would require Δ_D to vary with position on the body, but we will take Δ_D to be some average value for the whole body. Similarly, the value of the mean free path of the molecules near the body will depend on position on the body, but we will use a nominal or averaged mean free path, λ_2, for the gas between the shock wave and the body.

According to our model, we can sum the free-molecule and continuum drags and obtain

$$C_D q_\infty A = C_{DFM} q_{\infty FM} A + C_{DC} q_{\infty C} A \tag{C33a}$$

$$C_D = C_{DFM} \left(\frac{q_{\infty FM}}{q_\infty} \right) + C_{DC} \left(\frac{q_{\infty C}}{q_\infty} \right) \tag{C33b}$$

The dynamic pressure ratios are evaluated as density or mass fraction ratios:

$$\frac{q_{\infty FM}}{q_\infty} = \frac{\rho_{\infty FM}}{\rho_\infty} = e^{-\Delta_D/\lambda_2} \tag{C34a}$$

$$\frac{q_{\infty C}}{q_\infty} = \frac{\rho_{\infty C}}{\rho_\infty} = 1 - e^{-\Delta_D/\lambda_2} \tag{C34b}$$

Combining equations (C34) with (C33b), we have

$$C_D = C_{DC} + (C_{DFM} - C_{DC}) e^{-\Delta_D/\lambda_2} \tag{C35}$$

We can insert the quantity, E_ϑ, from equation (58) into equation (C35) to obtain

$$C_D = C_{DC} \left(1 + E_\vartheta e^{-\Delta_D/\lambda_2} \right) \tag{C36}$$

We observe that equations (C35) and (C36) have the correct asymptotes. The variable, Δ_D/λ_2, is a reciprocal Knudsen number. To this point, the derivation is similar to that found in reference 34, but from a somewhat different point of view. In reference 34, Δ_D is specified as the shock standoff distance, evaluated empirically in terms of ρ_{21} and R for a sphere; this reciprocal Knudsen number is then multiplied by a constant factor to fit experimental data.

We can postulate a functional form for Δ_D as

$$\Delta_D = f_\alpha(R,\ Re_\infty,\ M_\infty,\ \text{body shape})$$

From dimensional considerations, we write

$$\Delta_D = Rf_\beta(Re_\infty,\ M_\infty,\ \text{body shape})$$

where the nose radius, R, characterizes the body size. Then we have

$$\frac{\Delta_D}{\lambda_2} = \frac{R}{\lambda_2} f_\beta \tag{C37a}$$

We can write

$$\frac{\Delta_D}{\lambda_2} = \frac{R\rho_{21}(D\ 10^{-6})f_\beta}{\lambda_2\rho_2} \tag{C37b}$$

This latter form is equivalent to the exponent in equation (7) of reference 34 when $\rho_{21}f_\beta$ is taken as a constant for a spherical body shape. As shown in reference 34, with the constant properly adjusted, a good fit is obtained with the drag data for a sphere at high speeds in air and in helium.

For practical calculations, it seems preferable to avoid evaluating λ_2. We can use the classical relation between viscosity and mean free path (eq. (119) of ref. 27) which states that viscosity is proportional to the product of $\lambda\rho$ and a mean molecular speed. We can express $\lambda_2\rho_2$ in terms of an undissociated value, $\lambda_{2u}\rho_{2u}$; this involves using $f_\mu(p_{t_2},\ T_s)$, the ratio of actual viscosity to the undissociated (Sutherland) viscosity. (Values of f_μ for air are tabulated in table VI of ref. 35.) We make use of the Sutherland formula,

$$\frac{\mu}{\mu_\infty} = \sqrt{\frac{T}{T_\infty}}\left[\frac{1 + (b/T_\infty)}{1 + (b/T)}\right] \tag{C38}$$

to relate to free-stream conditions, and we obtain the approximation

$$\lambda_2\rho_2 = \lambda_\infty\rho_\infty\sqrt{\frac{m_2}{m_\infty}}\left[\frac{T_s + b(T_s/T_\infty)}{T_s + b}\right] f_\mu \tag{C39}$$

Using equation (106) of reference 27, we can write

$$\lambda_\infty \rho_\infty = \frac{K_\lambda m_\infty}{S_\infty} \tag{C40}$$

and put equation (C39) in the form

$$\lambda_2 \rho_2 = \frac{K_\lambda m_\infty}{S_\infty} \sqrt{\frac{m_2}{m_\infty}} \left[\frac{T_S + b(T_S/T_\infty)}{T_S + b} \right] f_\mu \tag{C41}$$

Substituting this expression into equation (C37b) we have

$$\frac{\Delta_D}{\lambda_2} = \frac{(RD)10^{-6}\rho_{21} f_\beta}{\frac{K_\lambda m_\infty}{S_\infty} \sqrt{\frac{m_2}{m_\infty}} \left[\frac{T_S + b(T_S/T_\infty)}{T_S + b} \right] f_\mu} \tag{C42}$$

We let

$$f_\gamma = \frac{10^{-6}\rho_{21} f_\beta}{\frac{K_\lambda m_\infty}{S_\infty} \sqrt{\frac{m_2}{m_\infty}} \left[\frac{T_S + b(T_S/T_\infty)}{T_S + b} \right] f_\mu} \tag{C43}$$

and we have

$$\frac{\Delta_D}{\lambda_2} = RD f_\gamma \tag{C44}$$

where

$$f_\gamma = f_\gamma (Re_\infty, M_\infty, \text{gas, body shape}) \tag{C45}$$

For given flight conditions and gas, f_γ will be a function of body shape (includes angle of attack). For many flight cases, body shape does not change much in the passage through the transitional regime; it can be expected that generally f_γ will not undergo a large variation in the transitional passage. We now approximate f_γ as a constant for the flight of a given body and use

$$f_\gamma = 15(1 + E_{14}) \tag{C46}$$

where E_{14} can be assigned the value zero for a sphere in air, and the constant, 15, has been selected to match experimental data as described below. We combine equations (C36), (C44), and (C46) to obtain our drag bridging equation.

$$C_D = C_{DC} \left[1 + E_9 e^{-15(RD)(1+E_{14})} \right] \tag{57}$$

The parameter, E_{14}, can be adjusted, in principle, to account approximately for the effects of all the variables in equation (C45) (during passage through the transitional regime). Unless data are at hand, E_{14} for air would normally be assigned the value zero, as for a sphere. Although the (presumably modest) dependence of E_{14} on body shape may not be known, the values of C_D calculated from equation (57) will also depend directly on body shape through C_{DC} and E_9. The constant, 15, in equations (C46) and (57) was determined by matching calculated values of drag with the measured drag data for spheres in air of reference 36. The comparison is shown in figure 9. Corresponding with calculated values of C_D for figure 9, the values of RD used in equation (57) were converted to Re_∞, because the data of reference 36 are plotted with Re_∞ as abscissa. The data of reference 36 were obtained in air at a nominal settling chamber temperature of 300° K over a Mach number range from 3.8 to 4.3. The data indicate that any Mach number effect on the transition of the drag coefficient is probably small. The value, $E_{14} = 0$ was also used to obtain a good fit with sphere drag data in air reported in reference 34 (not shown). One set of these data was obtained in undissociated air at a nominal settling chamber temperature of 2500° K over a Mach number range from 15.96 to 20.90. Another set of data was obtained in dissociated air over a range of hypersonic Mach numbers (11.34 to 58.7) at a nominal settling chamber temperature of 9000° K. A third set of sphere drag data was obtained in helium with hypersonic flow conditions. The helium data require $E_{14} \approx 2$ for a good fit.

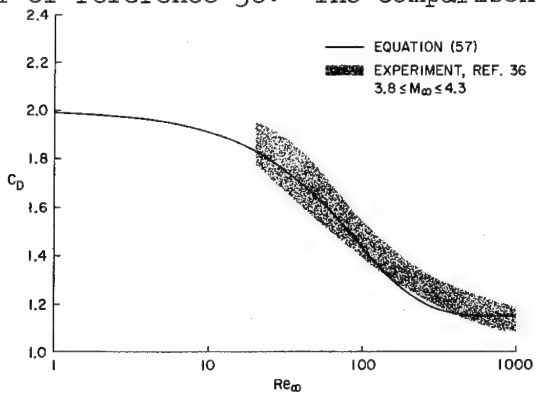

Figure 9.- Comparison of calculated and measured values of the drag coefficient for spheres in the transitional regime.

The drag coefficient, C_D, is used only in equation (59) for the quantity M/C_DA. Equation (59) contains an empirical evaluation of the variation of body mass, M, with the stagnation point surface recession, X. Any change in the continuum drag coefficient, C_{DC}, can also be accounted for in the empiricism of the M/C_DA evaluation.

Example of Free-Molecule-Continuum Bridging

The bridging relations developed in this appendix are essentially approximations to be used for the conditions for which they were derived. For other conditions, more rigorously developed equations may be available, as, for example, for cases of shear in Couette flow such as reported in reference 33. Under conditions for which no well developed bridging relations exist, the formulas given in this appendix are recommended as engineering approximations. The structure of these equations insures that the equations have the correct asymptotes, and this tends to limit inaccuracies.

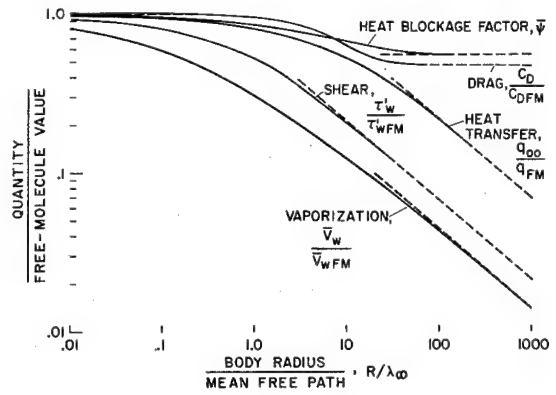

Figure 10.- Representative calculation of bridging between free-molecule and continuum flow.

Representative curves obtained from the bridging equations are presented in figure 10. The ordinate quantities, normalized to their free-molecule values, are plotted against a reciprocal Knudsen number which was varied by varying the nose radius, R. Although the bridging equations are general, the numerical inputs to the equations, and therefore the curves obtained, will depend on the individual case calculated. The calculated curves in the figure are for a tektite glass. A curve for the quantity $q_{\psi w}$ (eq. (18)) is not shown; this quantity is the product of the quantities, $\bar{\psi}$ and q_{∞} (see eq. (22b)), for which the curves are shown. The dotted lines on the right side of the figure are the continuum regime asymptotes for the various quantities, while on the left side the free-molecule asymptote for all quantities is unity. It is noted that the various quantities approach their asymptotes at different rates. (Under some conditions, one can consider that all of the quantities plotted are not even in the same regime.) The figure illustrates probably the most important feature of the bridging relations used. They automatically place control of the various quantities in the appropriate controlling regime, the free-molecule, transitional, or continuum.

Curves corresponding to those of figure 10 can be plotted for other materials, and most of the curves will be similar, but somewhat displaced. The heat transfer curve (q_{∞}) is approximately universal; the drag curve (C_D) is influenced considerably by body shape; the other curves (τ'_w, $\bar{v}_w$, $\bar{\psi}$) will vary somewhat with relative rates of vaporization (or reaction) of the material being considered.

APPENDIX D

USE OF COMPUTING PROGRAM

The computing program can be used to solve a variety of problems involving surface-type ablation. Data are arbitrarily read in subject to the limitations given below in the listing of Input Data. As explained in the section METHOD OF THE NUMERICAL PROGRAM, the stability parameter, Z, should be $\leq 1/2$ for all grid points and at all times. The quantity, Z, is printed out by the program so that its values may be observed.

Computing Program Options

The numerical computing program has six major groups of options as listed below.

1. Running conditions

   (a) Normal wind tunnel, KF = 1.

   (b) Rarefied wind tunnel, KF = 2.
   (includes all wind tunnel cases, but computing time is longer than with option (a))

   (c) Flight, KF = 3.

Both of the wind-tunnel options, (a) and (b), allow wind-tunnel conditions to be changed once, if desired, and also for the wind tunnel to be shut off. At time, t_{cha} (GAMAI), the free-stream density, enthalpy velocity, and free-stream velocity are changed, respectively, to D_{cha} (C7), V_{cha} (C8), and $V_{\infty cha}$ (OKBAR). At time, t_{off} (OMCO), the wind tunnel is shut off, and the calculations are continued while the model cools. If these changes are not desired, the values of t_{cha} and t_{off} can be set larger than the time corresponding to the final time line number, NF (see Time Sketch below).

2. Internal radiation

   (a) Transparent, KG = 1.

   (b) Opaque, KG = 2.

   (c) Semitransparent, KG = 3.

3. Surface conditions

   (a) Evaporation or sublimation, KCH = 1.

   (b) Surface chemical reaction, KCH = 2.

4. Initial conditions for flight case (KF = 3); (see appendix B).

   (a) Normal entry into an atmosphere using a computed exponential temperature profile in the body. With an assumed $T_{wi} (> T_o)$, the initial values, D_i and Δ_i are computed by the program, KDEL = 1.

   (b) Arbitrary initial values of atmospheric density, D_i, and thermal thickness of exponential temperature profile in the body, Δ_i, KDEL = 2.

5. Back face boundary conditions

   (a) Back face aerodynamically exposed, KBAK = 1.

   (b) Backing material forming a heat sink, KBAK = 2. (For a heat sink of zero heat capacity, or an adiabatic back boundary, KBAK = 1 should be used.)

6. Planet and atmosphere for flight case (KF = 3)

   (a) Earth entry with the ARDC atmosphere (approximated exponentially with 3 programmed values of scale height). Earth radius programmed at 6440 km (R_p in eq. (53)), KC5 = 1.

   (b) Arbitrary planet with exponential atmosphere having arbitrary scale height (initial, two intermediate, and final values), KC5 = 2.

Nomenclature of Computing Program

The nomenclature used in the computing program is in symbolic FORTRAN language. Separate listings of input and output data are shown below.

Input Data

Input data are listed below in their order of card punching. Actual card formats are shown in the Input Card Format Sketch. All input data are printed out by the program in an initial readout (see Sample Case, below). A quantity listed as an option is defined in the section, Computing Program Options, above.

Following the definition of a quantity, the value of an option selection may be shown. The particular quantity is not needed (and not used) for other values of the option selection. Unused quantities are normally assigned the value zero; in any case, the input card formats must be maintained.

The maximum number of grid points to be used in the finite difference spacing is 98; this is the maximum value for the quantity, MF (see Spacing Sketch).

4	8	12	16	20	24	28	32	36	40	44	48	52	56	60	64	68	72	CARD
KF	KG	N1	N2	NF	K2	K3	K4	LN	M2	M3	MF	J1	J2	KC5	KCT	KM1	KM2	A
KM3	KCM1	KCM2	KCM3	KCMF	KN1	KN2	KCN1	KCN2	KCNF	KCH	KDEL	KBAR						B

ALL NUMBERS IN I4 FORMAT (MUST BE RIGHT JUSTIFIED)

1	10	19	28	37	46	55	64	72	
A1	A2	A3	A4	B1	B2	B3	B4		1
B5	B6	B7	B8	B9	B10	B11	B12		2
B13	B14	B15	B16	C1	C2	C3	C4		3
C5	C6	C7	C8	E1	E2	E3	E4		4
E5	E6	E7	E8	E9	E10	E11	E12		5
E13	E14	E15	E16	SIGMA	RO	OMCO	OKBAR		6
CHII	VCINF)	GAMA1	TW1	DELTW	ALLOW	HS	DC1		7
DTT1	DTT2	DTT3	DY1	RHO21	OMO	E17	E18		8
DELTJ	E19	RB	E20	E21	E22	E23	E24		9
E25	E26	E27	E28	E29	E30	E31	E32		10
E33	E34	E35	E36	E37	E38	E39 (OPEN)	E40 (OPEN)		11

ALL NUMBERS IN E9.3 FORMAT (DECIMAL POINT NEEDED)

1	10	19	28 36	40	72	
ALPHA	ALPHA2	EMAX	RN	IT		12
(E9.3)	(E9.3)	(E9.3)	(E9.3)	(I4)		

FORMATS ARE INDICATED BY PARENTHESES. E FORMATS REQUIRE DECIMAL POINT. I FORMAT MUST BE RIGHT JUSTIFIED.

Input Card Format Sketch

NI, N2 ARE BREAK POINTS FOR CHANGING Δt

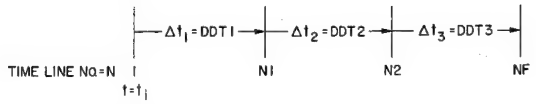

Δt_1, Δt_2, Δt_3, ARE INCREMENTS USED IN FINITE DIFFERENCE EQUATION

Time Sketch

M1, M2, M3 ARE BREAK POINTS FOR CHANGING $\Delta\eta$

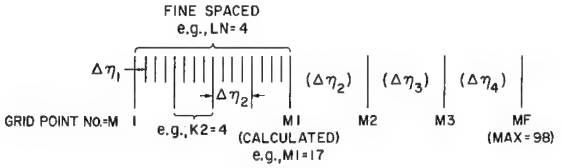

INITIALLY $\Delta Y_i = \Delta\eta_i$

$\Delta\eta_2$, $\Delta\eta_3$, $\Delta\eta_4$ ARE INCREMENTS USED IN FINITE DIFFERENCE EQUATION

$\Delta\eta_1$ INCREMENT USED FOR INTERPOLATIONS

INITIAL VALUE OF LENGTH/$\Delta\eta_1 \leq 1665$ REQUIRED FOR TRANSPARENT CASE (KG=1)

Spacing Sketch

ONE TIME LINE

KMI, KM2, KM3 ARE BREAK POINTS FOR PRINTING INCREMENTS

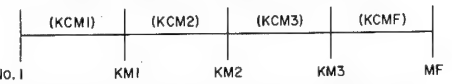

KCMI, KCM2, KCM3, KCMF ARE GRID-POINT PRINTING INCREMENTS

BETWEEN TIME LINES

KNI, KN2 ARE BREAK POINTS FOR PRINTING INCREMENTS

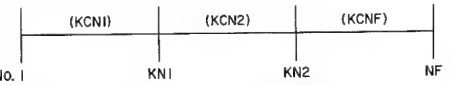

KCNI, KCN2, KCNF ARE TIME LINE PRINTING INCREMENTS

Printing Sketch

Card A

(All numbers are integers in I4 FORMAT)

KF Running condition option

KG Internal radiation option

N1 Time line number at which the finite time increment Δt (DTT) changes from Δt_1 (DDT1) to Δt_2 (DDT2) (see Time Sketch).

N2 Time line number at which the finite time increment Δt (DTT) changes from Δt_2 (DDT2) to Δt_3 (DDT3) (see Time Sketch).

NF Final time line number (see Time Sketch).

K2 Defined by $\Delta\eta_2 = (K2)\,\Delta\eta_1$ (or $\Delta y_2 = (K2)\,\Delta y_1$). Can be 1 for opaque and semitransparent cases (KG = 2, 3), but must be at least 2 and even for transparent case (KG = 1) (see Spacing Sketch).

K3 — Defined by $\Delta\eta_3 = (K3)\ \Delta\eta_2$ (or $\Delta y_3 = (K3)\ \Delta y_2$). Can be 1 (see Spacing Sketch).

K4 — Defined by $\Delta\eta_4 = (K4)\ \Delta\eta_3$ (or $\Delta y_4 = (K4)\ \Delta y_3$). Can be 1 (see Spacing Sketch).

LN — Increments of $\Delta\eta_2$ spacing over which $\Delta\eta_1$ spacing exists. Must be ≥ 4 (see Spacing Sketch).

M2 — Grid point at which space increment changes from $\Delta\eta_2$ to $\Delta\eta_3$ (see Spacing Sketch).

M3 — Grid point at which space increment changes from $\Delta\eta_3$ to $\Delta\eta_4$ (see Spacing Sketch).

MF — Grid point at back face. Maximum value = 98 (see Spacing Sketch).

J1 — Order of interpolation for T (TE) in the fine spaced ($\Delta\eta_1$) region.

J2 — Order of interpolation for Δ_μ (YDEL).

KC5 — Planet and atmosphere option for flight case (KF = 3).

KCT — Maximum number of iterations to determine front face temperature, T_w, within allowable error selected (ALLOW). If exceeded, calculation will stop.

KM1 — Grid point at which printing interval on one time line changes from KCM1 to KCM2 (see Printing Sketch).

KM2 — Grid point at which printing interval on one time line changes from KCM2 to KCM3 (see Printing Sketch).

Card B

(All numbers are integers in I4 FORMAT)

KM3 — Grid point at which printing interval on one time line changes from KCM3 to KCMF (see Printing Sketch).

KCM1, KCM2, KCM3, KCMF — Printing intervals of grid points (see Printing Sketch).

KN1 — Time line number at which time line printing interval changes from KCN1 to KCN2 (see Printing Sketch).

KN2 — Time line number at which time line printing interval changes from KCN2 to KCNF (see Printing Sketch).

KCN1,KCN2, KCNF	Time line printing intervals (see Printing Sketch).
KCH	Surface condition option.
KDEL	Initial condition option for flight case (KF = 3).
KBAK	Back face boundary condition option.

For cards 1-11, there are normally 8 numbers per card, each number in E9.3 FORMAT.

Card 1

A1	A_1, equation (27)	B1	ρ
A2	A_2, equations (10),(11)	B2	B_2, equation (84)
A3	A_3, equations (32),(35)	B3	B_3, equation (84)
A4	A_4, equation (15)	B4	B_4, equation (85)

Card 2

B5	B_5, equation (85)	B9	B_9, equation (87)
B6	B_6, equation (86)	B10	$\bar{M}$, equation (29)
B7	B_7, equation (86)	B11	B_{11}, equations (28), (30)
B8	T_o	B12	h_v

Card 3

B13	ϵ_{FF} for opaque case (KG = 2); ϵ_{max} for semitransparent case (KG = 3)
B14	B_{14}, equation (85)
B15	ϵ_{BF} for opaque and semitransparent cases (KG = 2, 3)
B16	B_{16}, equations (46), (47), (51); B_{16} = 1 for transparent case (KG = 1); B_{16} = 0 for opaque and semitransparent cases (KG = 2, 3)
C1	C_1, equation (60)
C2	C_2, equation (60)
C3	C_3, equations (56), (59)
C4	C_4, equations (56), (59)

Card 4

C5 Sh_1, for flight case (KF = 3), and (KC5 = 2).

C6 C_6, equation (15)

C7 L/D_r, equation (53) for flight case (KF = 3); D_{cha} for wind tunnel cases (KF = 1, 2).

C8 $g_p/10^5$, equation (53b) for flight case (KF = 3); V_{cha} for wind tunnel cases (KF = 1, 2).

E1 E_1, equation (86)

E2 E_2, equation (87)

E3 E_3, equation (88)

E4 E_4, equation (44)

Card 5

E5 E_5, equation (44)

E6 E_6, equation (44)

E7 E_7, equation (26)

E8 E_8, equations (34), (35)

E9 E_9, equation (58)

E10 E_{10}, equation (88)

E11 E_{11}, equation (61)

E12 E_{12}, equation (61)

Card 6

E13 E_{13}, equation (50)

E14 E_{14}, equations (57), (59)

E15 E_{15}, equation (10a)

E16 E_{16}, equation (12)

SIGMA $\sigma = 1.369 \times 10^{-12}$

RO R_i, equation (60)

OMCO $(M/C_{DC}A)_i$, equation (59) for flight case (KF = 3); t_{off} for wind tunnel cases (KF = 1, 2).

OKBAR $\bar{K}$, equation (12) for flight case (KF = 3); $V_{\infty cha}$ for wind tunnel cases (KF = 1, 2).

Card 7

CHI1 χ_1, equation (12)

VCINFI $V_{\infty i}$ for flight case (KF = 3); for wind tunnel cases (KF = 1, 2), V_∞ = VCINFI until $t > t_{cha}$ or $t > t_{off}$.

GAMAI γ_i for flight case (KF = 3); t_{cha} for wind tunnel cases (KF = 1, 2).

TWI T_{wi}; $> T_o$ for entry flight case (KF = 3, KDEL = 1).

DELTW Initial guess for incrementing T_{wi} in iterating for T_w in the second time line (can be zero).

ALLOW e_{al}

HS h_s for wind tunnel cases (KF = 1, 2); constant at read-in value until $t > t_{cha}$ or $t > t_{off}$.

DCI D_i for flight case (KF = 3); read in only when KDEL = 2; with KDEL = 1, D_i is calculated by the program. For wind tunnel cases (KF = 1, 2), read in; D = DCI until $t > t_{cha}$ or $t > t_{off}$.

Card 8

DDT1 Δt_1 (see Time Sketch).

DDT2 Δt_2 (see Time Sketch).

DDT3 Δt_3 (see Time Sketch).

DY1 $\Delta\eta_1$ = initial value of Δy_1 (see Spacing Sketch); initial value of length/$\Delta\eta_1 \leq 1665$ is required for the transparent case (KG = 1).

RHO21 ρ_{21}; read in for wind tunnel cases (KF = 1, 2); for flight case (KF = 3), ρ_{21} is calculated continuously (eq. (61)).

OMO $R_{B/F}$, equation (48); used only when back face is aerodynamically exposed (KBAK = 1).

E17 E_{17}, equation (60)

E18 E_{18}, equations (56),(59), used for flight case (KF = 3).

Card 9

DELTJ Initial guess for incrementing T_w in iteration for time lines 3, 4, 5; should not be zero.

E19 E_{19}, equation (49); used when back face is aerodynamically exposed (KBAK = 1).

RB — R_b, equations (48), (50); used when back face is aerodynamically exposed (KBAK = 1).

E20 — E_{20}, equation (87)

E21 — A_{cq}, equation (17), (KF = 2, 3); if unknown use $A_{cq} = 1$.

E22 — A_{cm}, equation (36), (KF = 2, 3); if unknown use $A_{cm} = 1$.

E23 — A'_{cv}, equations (39c, 39d), (KCH = 1); if unknown, evaluate using $A_{cv} = 1$ in equation (39c).

E24 — B, equation (39e), (KCH = 2).

Card 10

E25 — E_T, equation (39e), (KCH = 2).

E26 — $\overline{c}$, equation (51), (KBAK = 2); (if $\overline{c} = 0$, use KBAK = 1 and OMO = 0).

E27 — R_p, equation (53), flight case (KF = 3), and (KC5 = 2).

E28 — $\overline{\rho}_{\infty 2}$, flight case (KF = 3), and (KC5 = 2).

E29 — $\overline{\rho}_{\infty 3}$, flight case (KF = 3), and (KC5 = 2).

E30 — S_{h_2}, flight case (KF = 3), and (KC5 = 2).

E31 — S_{h_3}, flight case (KF = 3), and (KC5 = 2).

E32 — S_{h_i}, in equation (B10), flight case (KF = 3); used only when KDEL = 1 and KC5 = 2; has arbitrary value, but may equal S_{h_1} (C5).

Card 11

E33 — E_{33}, equation (45), semitransparent case (KG = 3).

E34 — Δ_i, in equation (B1); read in only for flight case (KF = 3), with arbitrary initial conditions (KDEL = 2). Otherwise the program computes Δ_i from equation (B2b).

E35 — E_{35}, equation (28)

E36 — E_{36}, transparent case (KG = 1); equation (97); $E_{36} = 1.0$ has given good energy balances.

E37 — E_{37}, transparent case (KG = 1); equation (98); $E_{37} = 1.0$ has given good energy balances.

E38 — E_{38}, flight case (KF = 3); equation (55).

E39,E40 (Open)

Card 12

This card is only required for the transparent case (KG = 1). The format for this card is shown in the Input Card Format Sketch. The FORTRAN quantities ALPHA, ALPHA2, EMAX, RN are in FORMAT E9.3; IT is in FORMAT I4.

ALPHA α, equation (41)

ALPHA2 α_2, equation (41)

EMAX ϵ_{max}, equation (42)

RN n, equations (41, 42)

IT Spacing of calculation and printing of F and $g = \partial F/\partial y$ in the fine spaced region (see Spacing Sketch). IT must be an integer factor of K2 but must be less than K2; for example, if K2 = 6, IT can be 1, 2, or 3. IT = 3 means that F and g are printed out for every third grid point in the fine spaced region; in the remaining regions they are printed for every grid point. The value of IT affects somewhat the accuracy of the finite difference and energy balance calculations. IT = 1 gives the greatest accuracy. A larger value of IT decreases accuracy while reducing computing time.

Output Data

All input data are printed out in an initial output format (see Sample Case below). In addition, the following quantities (some calculated) are printed in an initial output (see Sample Case below).

Q01I q_{wi}

Q02I q_{Ri}

Q0I q_{wRi}

TTI t_i; equation (B4) for wind tunnel cases (KF = 1, 2); equals zero for flight case (KF = 3).

DELI Δ_i; equation (B2b) for wind tunnel cases (KF = 1, 2) and flight case (KF = 3) with KDEL = 1; for flight case with KDEL = 2, Δ_i equals E34.

DCI D_i; read in quantity for wind tunnel cases (KF = 1, 2) and flight case (KF = 3) with KDEL = 2; from equation (B10) for flight case with KDEL = 1.

RHO $\bar{\rho}_\infty = D/1226$ (for this printing $D = D_i$).

M1 M1 = 1 + (K2)(LN); see Spacing Sketch.

The spacing of printing intervals is arbitrarily selected (see subsection Input Data and the Printing Sketch). For each time line printed out, the following quantities appear. (See section, Sample Case, below for format.)

N	N, time line number	OMC	M/C_DA
TT	t	XIP	$\overline{v}_{sr} = dX/dt$
R	R	CHI	X
SNGMA	$\sin \gamma$	DTT	Δt
RHO	$\overline{\rho}_\infty$	PDP	ρ''
VC	V	P	P
VCINF	V_∞	PHI	φ
PSI	ψ	A2D	A_{2D}
PSIBAR	$\overline{\psi}$	FBAR	$\overline{F}$
QOC	q_{oc}	FINT	$\overline{F}_t$
QOFM	q_{FM}	ADGABS	a_{Dg}
QO	q_o	AGABS	a_g
QOO	q_{oo}	EPSRER	ϵ_{BF}
PSQOO	$q_{\psi w}$	EPSLN	ϵ_{FF}
CKTU	$\overline{K}_{tu}$	FRS	F_{RS}
PSQOF	q_w	PT2	p_{t_2}
QR	q_R	COIN	Q_{con}
TDEL	Δ	RIN	Q_{rad}
YDEL	Δ_μ	VAP	Q_{vap}
TMDL	$T_{\Delta\mu}$	STOR	Q_{stor}
RHO21	ρ_{21}	VCON	Q_{vcon}
TAUCP	τ'_{wc}	UCON	Q_{ucon}
TAUFMP	τ'_{wFM}	RESID	Q_{res}
TAUWP	τ'_w	ERR	e_{rr}

DTDYW	$\left(\frac{\partial T}{\partial y}\right)_w$
PSQO	q_{con}
FRW	q_{rad}
DVAP	q_{vap}
DSTOR	q_{stor}, except at $t = t_i$, when DSTOR = (stored energy at t_i)/Δt; stored energy at t_i = absolute value of second term in equation (82d).
VARG	q_{vcon}
YTNT	q_{ucon}
DRES	q_{res}
KC	KC, number of iterations required to obtain T_w.
TW	T_w
VWC	$\lvert\overline{v}_{wc}\rvert$
VWFM	$\lvert\overline{v}_{wFM}\rvert$
VW	$\overline{v}_w$

Also for each time line, the following arrayed quantities print out in columns for the selected print spacing of grid points (see Printing Sketch and Sample Case below for format).

M	M (grid point number)
Y	y
TE	T
UDB	$\overline{\overline{u}}$
VBAR	$\overline{v}$
XRAT	X_r
G	g
FR	F
Z	Z, must be $\leq 1/2$ for stability.

Sample Case

To illustrate the use of the computing program, a sample case has been selected which describes the entry of a transparent tektite into the Earth's atmosphere. Figure 11 shows the input data for the sample case; figure 12 shows the printing out of the input data and the initial calculated values; figure 13 shows the printing out for a typical time line.

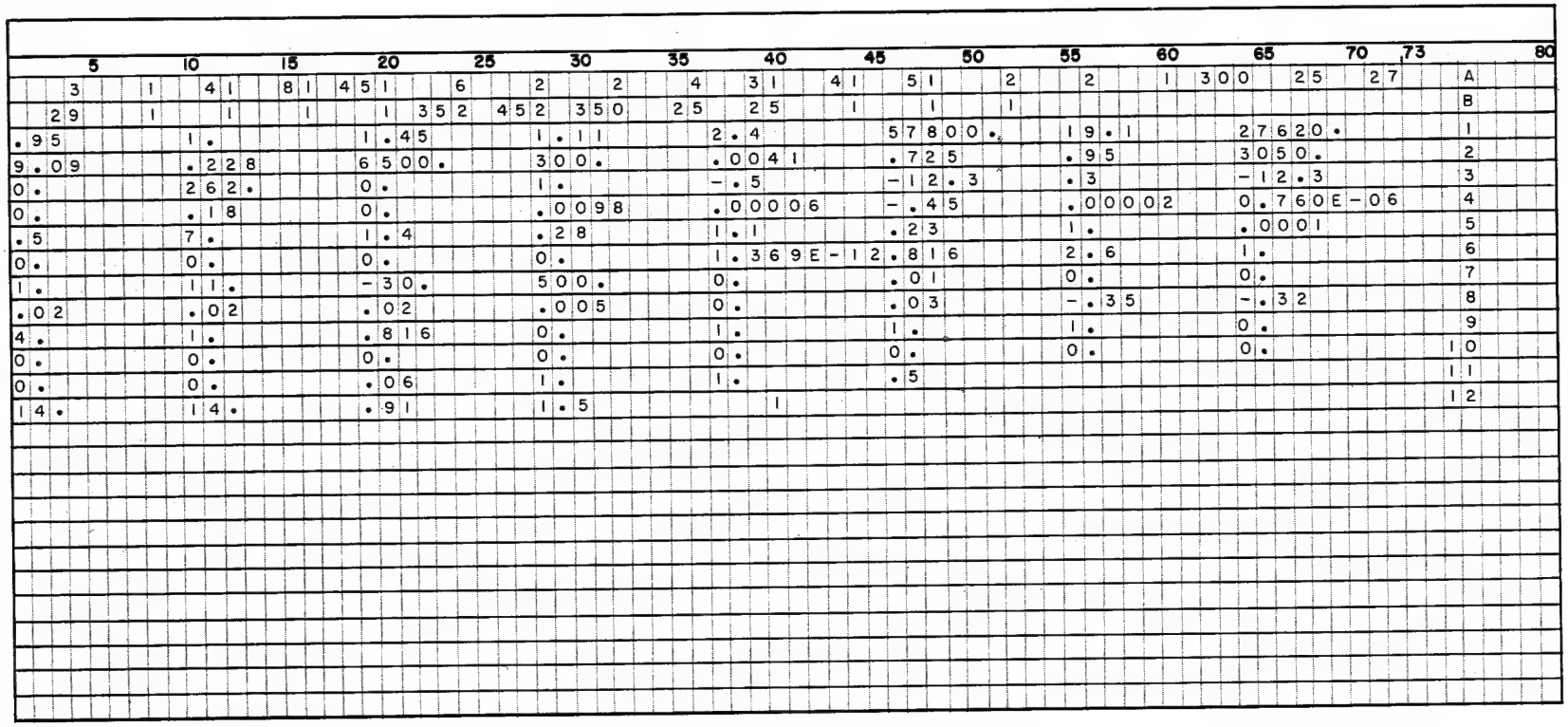

Figure 11.- Input data for sample case.

```
    A1          A2          A3          A4          B1          B2          B3          B4          B5
    B6          B7          B8          B9          B10         B11         B12         B13         B14
    B15         B16         C1          C2          C3          C4          C5          C6          C7
    C8          E1          E2          E3          E4          E5          E6          E7          E8
    E9          E10         E11         E12         E13         E14         E15         E16         SIGMA
    R3          OMCO        OKBAR       CHI1        VCINFI      GAMAI       TWI         DELTW       ALLOW
    HS          DCI         DDT1        DDT2        DDT3        DY1         RHO21       OM3           E17
    E18         DELTJ       E19         R8          E23         E21         E22         E23         E24
    E25         E26         E27         E28         E29         E30         E31         E32         E33
    E34         E35         E36         E37         E38         E39         E40
 0.95000E 00  0.10300E 01  0.14500E 01  0.11100E 01  0.24000E 01  0.57800E 05  0.19100E 02  0.27620E 05  0.93900E 01
 0.22800E-00  0.65000E 04  0.30000E 03  0.41000E-02  0.72500E 00  0.95200E 00  0.33500E 04 -0.          0.25200E 03
-0.           0.10000E 01 -0.50000E 00 -0.12300E 02  0.30000E-00 -0.12300E 02  0.          0.18000E-00  0.
 0.98000E-02  0.60000E-04 -0.45000E-00  0.26000E-04  0.76000E-06  0.50000E 00  0.70000E 01  0.14000E 01  0.28000E-00
 0.11000E 01  0.23000E-00  0.10000E 01  1.00000E-04  0.           -0.          0.          0.          0.13690E-11
 0.81600E 00  0.26000E 01  0.10000E 01  0.10000E 01  0.11000E 02 -0.30000E 02  0.50000E 03  0.          1.00000E-02
 0.           0.           0.20000E-01  0.20000E-01  0.20000E-01  0.50000E-02  0.          0.30000E-01 -0.35000E-00
-0.32000E-00  0.40000E 01  0.10000E 01  0.81600E 00 -0.           0.10000E 01  0.10000E 01  0.10000E 01 -0.
-0.          -0.          -0.          -0.          -0.          -0.          -0.          -0.          -0.
-0.           0.69000E-01  0.10000E 01  0.10000E 01  0.50000E 00 -0.          -0.          -0.          -0.
 KF   KG   N1   N2   NF   K2   K3   K4   LN   M2   M3   MF   J1   J2   KC5  KCT  KM1  KM2  KM3  KCM1 KCM2 KCM3 KCMF
KN1  KN2  KCN1 KCN2 KCNF  KCH KDEL KBAK
  3    1   41   81  451    6    2    2    4   31   41   51    2    2    1  303   25   27   29    1    1    1    1
352  452  350   25   25    1    1    1
    QQ1I        QQ2I        QQI         TTI         DELI        DCI         RHO         M1
 0.75471E 01  0.26723E-00  0.78143E 01  0.          0.84801E-01  0.47503E-03  0.38746E-06   25
ALPHA    ALPHA2     EMAX       RN        IT
14.000    14.000    0.910     1.500     1
```

Figure 12.- Print-out of input data and initial calculated values for sample case.

```
     N           TT          R          SNGMA       RHO         VC          VCINF       PSI         PSIBAR
   QCC         QOFM        QO          QOO         PSQOO       CKTU        PSQOF       QR          TDEL
  YDEL        TMDL        RHO21       TAUCP       TAUFMP      TAUWP       OMC         XIP         CHI
 DTT          PDP         P           PHI         A2D         FBAR        FINT        ADGABS      AGABS
  EPSRER      EPSLN       FRS         PT2         COIN        RIN         VAP         STOR        VCON
   UCON       RESID       ERR          DTDYW      PSQO        FRW         DVAP        DSTOR        VARG
   YTNT       DRES        KC          TW          VWC         VWFM        VW

       451         9.000  0.11480E 01 -0.49531E-00  0.43194E-03  0.82868E 01  0.82566E 01  0.63738E 00  0.63955E 00
0.57504E 03  0.32453E 04  0.57300E 03  0.57300E 03  0.36646E 03  0.10000E 01  0.36646E 03  0.17039E 01  0.51588E-01
0.49881E-02  0.25649E 04  0.14784E 02  0.14973E 05  0.31446E 06  0.14973E 05  0.13942E 01  0.13009E-00  0.51589E 00
0.20000E-01  0.27718E 06  0.15126E 01  0.30323E 01  0.18438E-00  0.13764E-00  0.15349E-00  0.13211E 03  0.13211E 03
0.87250E 06  0.26334E-00  0.21358E 02  0.34104E-02  0.17573E 04 -0.12594E 03 -0.57964E 03  0.22147E 03  0.13997E 03
0.70396E 03 -0.13639E 02 -0.51881E-02 -0.47963E 05  0.38467E 03 -0.23915E 02 -0.13107E 03  0.47626E 01  0.33219E 02
0.19381E 03  0.77705E 00           1  0.27743E 04  0.18762E-01  0.39214E-00 -0.17905E-01
         M           Y          TE          UDB          VBAR         XRAT          G           FR          Z
         1          0.       2774.333  0.11592E 02 -0.17905E-01  0.36834E 01  0.73194E 04 -0.19654E 02  0.
         2          0.004    2612.848  0.61359E 01 -0.77043E-01  0.17046E 01  0.46337E 04  0.24976E 01  0.
         3          0.008    2462.054  0.24586E 01 -0.11511E-00  0.10624E 01  0.31651E 04  0.16815E 02  0.
         4          0.011    2321.952  0.55968E 00 -0.13211E-00  0.89170E 00  0.20567E 04  0.26822E 02  0.
         5          0.015    2192.542  0.43912E-00 -0.12804E-00  0.10083E 01  0.12622E 04  0.32724E 02  0.
         6          0.019    2073.823  0.48401E-01 -0.13333E-00  0.99880E 00  0.69544E 03  0.36639E 02  0.
         7          0.023    1965.796  0.70356E-01 -0.12981E-00  0.10011E 01  0.29645E 03  0.38181E 02 -0.18238E-00
         8          0.026    1868.460  0.21479E-02 -0.13012E-00  0.99988E 00  0.21975E 02  0.39023E 02  0.
         9          0.030    1781.816  0.11390E-01 -0.13004E-00  0.10012E 01 -0.16227E 03  0.38460E 02  0.
        10          0.034    1725.863  0.54371E-03 -0.13009E-00  0.10006E 01 -0.27715E 03  0.37886E 02  0.
                    0.038    1640.602                -0.13008E-00                -0.34385E 03                0.
```

Figure 13.- Print-out of a typical time line for sample case.

REFERENCES

1. Chapman, Dean R.; and Larson, Howard K.: On the Lunar Origin of Tektites. J. Geophys. Res., vol. 68, no. 14, July 15, 1963, pp. 4305-4358.

2. Chapman, Dean R.: On the Unity and Origin of the Australasian Tektites. Geochim. et Cosmochim. Acta, vol. 28, no. 6, June 1964, pp. 841-880.

3. Landau, H. G.: Heat Conduction in a Melting Solid. Quart. Appl. Math., vol. 8, no. 1, April 1950, pp. 81-94.

4. Lotkin, Mark: The Calculation of Heat Flow in Melting Solids. Quart. Appl. Math., vol. 18, no. 1, April 1960, pp. 79-85.

5. Fledderman, R. G.; and Hurwicz, H.: Transient Ablation and Heat-Conduction Phenomena at a Vaporizing Surface. AVCO Tech. Rep. RAD TR-9(7)-60-9.

6. Adams, Ernst W.: Theoretical Investigations of the Ablation of a Glass-Type Heat Protection Shield of Varied Material Properties at the Stagnation Point of a Re-entering IRBM. NASA TN D-564, 1961.

7. Detra, R. W.; Kemp, N. H.; and Riddell, F. R.: Addendum to Heat Transfer to Satellite Vehicles Re-entering the Atmosphere. Jet Propulsion, vol. 27, no. 12, Dec. 1957, pp. 1256-1257.

8. Hayes, Wallace D.; and Probstein, Ronald F.: Hypersonic Flow Theory. Academic Press, N. Y., 1959.

9. Hidalgo, Henry: Ablation of Glassy Material Around Blunt Bodies of Revolution. ARS J., vol. 30, no. 9, Sept. 1960, pp. 806-814.

10. Hoshizaki, H.: Mass Transfer and Shock Generated Vorticity. ARS J., vol. 30, no. 7, July 1960, pp. 628-634.

11. Spalding, D. B.: The Theory of Melting Ablation, With Vaporization, Gas-Phase Chemical Reaction, Surface Pyrolysis, and Transient Effects. Aero. Quart., vol. 12, pt. 3, Aug. 1961, pp. 237-274.

12. Reshotko, Eli; and Cohen, Clarence B.: Heat Transfer at the Forward Stagnation Point of Blunt Bodies. NACA TN 3513, 1955.

13. Baron, Judson R.: The Binary Mixture Boundary Layer Associated With Mass Transfer Cooling at High Speeds. MIT Naval Supersonic Lab., Tech. Rep. 160, May 1956.

14. Kadanoff, Leo P.: Radiative Transport Within an Ablating Body. Trans. ASME, J. Heat Transfer, vol. 83, no. 2, May 1961, pp. 215-225.

15. Gardon, Robert: A Review of Radiant Heat Transfer in Glass. J. Am. Ceramic Soc., vol. 44, no. 7, July 1961, pp. 305-312.

16. Kourganoff, V.: Basic Methods in Transfer Problems; Radiative Equilibrium and Neutron Diffusion. Clarendon Press, Oxford, 1952.

17. James, Carlton S.: Experimental Study of Radiative Transport From Hot Gases Simulating in Composition the Atmospheres of Mars and Venus. AIAA J., vol. 2, no. 3, March 1964, pp. 470-475.

18. Chapman, Dean R.: An Approximate Analytic Method for Studying Entry Into Planetary Atmospheres. NASA TR R-11, 1959.

19. Hochstim, Adolf R.: Gas Properties Behind Shocks at Hypersonic Velocities, I, Normal Shocks in Air. Convair Rep. ZPh(GP)-002, Astia Document AD 134398, Jan. 30, 1957.

20. Hidalgo, Henry; and Kadanoff, Leo P.: Comparison Between Theory and Flight Ablation Data. AIAA J., vol. 1, no. 1, Jan. 1963, pp. 41-45.

21. Wentink, Tunis, Jr.: High Temperature Behavior of Teflon. Avco-Everett Res.Rep. 55, AF BMD-TN-59-15, 1959.

22. Madorsky, Samuel L.: Thermal Degradation of Organic Polymers. Interscience Pub., N. Y., 1964.

23. Lee, George; and Sundell, Robert E.: Apollo Afterbody Heat Transfer and Pressure With and Without an Ablating Teflon Nose Cap at M_∞ of 5.8 to 8.3. NASA TN D-3620, 1966.

24. Seiff, Alvin; and Reese, David E., Jr.: Defining Mars' Atmosphere - A Goal for the Early Missions. Astronautics and Aeronautics, vol. 3, no. 2, Feb. 1965, pp. 16-21.

25. Anon.: Astro Notes. Aeronautics and Astronautics, vol. 3, no. 11, Nov. 1965, pp. 106-111.

26. Carslaw, H. S.; and Jaeger, J. C.: Conduction of Heat in Solids. Oxford, 1947.

27. Kennard, Earle H.: Kinetic Theory of Gases With an Introduction to Statistical Mechanics. First ed, McGraw-Hill, N. Y., 1938.

28. Scala, S. M.; and Vidale, G. L.: Vaporization Processes in the Hypersonic Laminar Boundary Layer. Internat. J. Heat and Mass Trans., vol. 1, no. 1, June 1960, pp. 4-22.

29. Page, Leigh: Introduction to Theoretical Physics. Second ed., Van Nostrand, N. Y., 1935.

30. Matting, Fred W.: General Solution of the Laminar Compressible Boundary Layer in the Stagnation Region of Blunt Bodies in Axisymmetric Flow. NASA TN D-2234, 1964.

31. Ferri, Antonio; and Zakkay, Victor: Measurements of Stagnation Point Heat Transfer at Low Reynolds Numbers. J. Aero/Space Sci., vol. 29, no. 7, July 1962, pp. 847-850.

32. Sherman, Frederick S.: A Survey of Experimental Results and Methods for the Transition Regime of Rarefied Gas Dynamics. Rarefied Gas Dynamics, Proc. Third Internat. Symp. on Rarefied Gas Dynamics, J. A. Laurmann, ed., Academic Press, N. Y., 1963, pp. 228-260.

33. Yang, Hsun-Tiao; and Lees, Lester: Plane Couette Flow at Low Mach Number According to the Kinetic Theory of Gases. Proc. 5th Midwestern Conference on Fluid Mechanics, Ann Arbor, Mich., 1957, pp. 41-65.

34. Masson, David J.; Morris, Deane N.; and Bloxsom, Daniel E.: Measurements of Sphere Drag From Hypersonic Continuum to Free-Molecule Flow. Rarefied Gas Dynamics, Proc. Second Internat. Symp. on Rarefied Gas Dynamics, L. Talbot, ed., Academic Press, N. Y., 1961, pp. 643-661.

35. Hansen, C. Frederick: Approximations for the Thermodynamic and Transport Properties of High-Temperature Air. NASA TR R-50, 1959.

36. Wegener, Peter P.; and Ashkenas, Harry: Wind Tunnel Measurements of Sphere Drag at Supersonic Speeds and Low Reynolds Numbers. J. Fluid Mech., vol. 10, pt. 4, June 1961, pp. 550-560.

NASA-Langley, 1966 A-2418

"The aeronautical and space activities of the United States shall be conducted so as to contribute . . . to the expansion of human knowledge of phenomena in the atmosphere and space. The Administration shall provide for the widest practicable and appropriate dissemination of information concerning its activities and the results thereof."

—NATIONAL AERONAUTICS AND SPACE ACT OF 1958

NASA SCIENTIFIC AND TECHNICAL PUBLICATIONS

TECHNICAL REPORTS: Scientific and technical information considered important, complete, and a lasting contribution to existing knowledge.

TECHNICAL NOTES: Information less broad in scope but nevertheless of importance as a contribution to existing knowledge.

TECHNICAL MEMORANDUMS: Information receiving limited distribution because of preliminary data, security classification, or other reasons.

CONTRACTOR REPORTS: Technical information generated in connection with a NASA contract or grant and released under NASA auspices.

TECHNICAL TRANSLATIONS: Information published in a foreign language considered to merit NASA distribution in English.

TECHNICAL REPRINTS: Information derived from NASA activities and initially published in the form of journal articles.

SPECIAL PUBLICATIONS: Information derived from or of value to NASA activities but not necessarily reporting the results of individual NASA-programmed scientific efforts. Publications include conference proceedings, monographs, data compilations, handbooks, sourcebooks, and special bibliographies.

Details on the availability of these publications may be obtained from:

SCIENTIFIC AND TECHNICAL INFORMATION DIVISION

NATIONAL AERONAUTICS AND SPACE ADMINISTRATION

Washington, D.C. 20546